A fungal arrestin protein contributes to cell cycle progression and pathogenesis

Calla L. Telzrow,[a,b] Connie B. Nichols,[a] Natalia Castro-Lopez,[c] Floyd L. Wormley Jr.,[c]*
J. Andrew Alspaugh[a,b]#

[a]Department of Medicine, Duke University School of Medicine, Durham, NC
[b]Department of Molecular Genetics and Microbiology, Duke University School of Medicine, Durham, NC
[c]Department of Biology, University of Texas at San Antonio, San Antonio, TX
*Current address: Texas Christian University, Fort Worth, TX

Running Head: Arrestin proteins in *C. neoformans*

#Address correspondence to J. Andrew Alspaugh, andrew.alspaugh@duke.edu

Abstract word count: 231
Text word count: 5,955

ABSTRACT

Arrestins, a structurally specialized and functionally diverse group of proteins, are central regulators of adaptive cellular responses in eukaryotes. Previous studies on fungal arrestins have demonstrated their capacity to modulate diverse cellular processes through their adaptor functions, facilitating the localization and function of other proteins. However, the mechanisms by which arrestin-regulated processes are involved in fungal virulence remain unexplored. We have identified a small family of four arrestins - Ali1, Ali2, Ali3, and Ali4 - in the human fungal pathogen *Cryptococcus neoformans*. Using complementary microscopy, proteomic, and reverse genetic techniques, we have defined a role for Ali1 as a novel contributor to cytokinesis, a fundamental cell cycle-associated process. We observed that Ali1 strongly interacts with proteins involved in lipid synthesis, and that *ali1*Δ mutant phenotypes are rescued by supplementation with lipid precursors that are used to build cellular membranes. From these data, we hypothesize that Ali1 contributes to cytokinesis by serving as an adaptor protein, facilitating the localization of enzymes that modify the plasma membrane during cell division, specifically the fatty acid synthases, Fas1 and Fas2. Finally, we assessed the contributions of the *C. neoformans* arrestin family to virulence, to better understand the mechanisms by which arrestin-regulated adaptive cellular responses influence fungal infection. We observed that the *C. neoformans* arrestin family contributes to virulence, and that the individual arrestin proteins likely fulfill distinct functions that are important for disease progression.

IMPORTANCE

To survive in unpredictable conditions, all organisms must adapt to stressors by regulating adaptive cellular responses. Arrestin proteins are conserved regulators of adaptive cellular responses in eukaryotes. Studies that have been limited to mammals and model fungi have demonstrated that disruption of arrestin-regulated pathways is detrimental for viability. The human fungal pathogen *Cryptococcus neoformans* causes more than 180,000 infection-related deaths annually, especially among immunocompromised patients. In addition to being genetically-tractable, *C. neoformans* has a small arrestin family of four members, lending itself to a comprehensive characterization of its arrestin family. This study serves as a functional analysis of arrestins in a pathogen, particularly in the context of fungal fitness and virulence. We investigate the functions of one arrestin protein, Ali1, and define its novel contributions to cytokinesis. We additionally explore the virulence contributions of the *C. neoformans* arrestin family and find that they contribute to disease establishment and progression.

INTRODUCTION

Tight regulation of signal transduction pathways is necessary for appropriate cellular adaptation to the environment. Arrestins are a group of multifunctional proteins that modulate the activation and repression of diverse signaling pathways in eukaryotes (1–4). Structurally, arrestins are defined by protein domains with conserved β-sheet-rich regions, termed the N-terminal and C-terminal arrestin domains, that provide important secondary structure guiding protein localization and activity (5, 6). Functionally, arrestins link plasma membrane-initiated signals to intracellular responses by regulating signal internalization and intracellular signaling cascades. In doing so, arrestins enable the eukaryotic cell to fine-tune adaptive cellular responses through three specific mechanisms: desensitizing G protein-coupled receptors (GPCRs), scaffolding signaling cascades, and serving as adaptor proteins (1–4).

Nearly four decades ago, arrestins were first discovered for their unique ability to "arrest" cellular responses to persistent stimuli, in a classical process termed desensitization (7). Desensitization has been most commonly reported for and most extensively explored in visual and β-arrestins, classes of arrestins that are specific to metazoan cells (7–9). A third class of arrestins, the α-arrestins, are the evolutionary predecessors of the visual and β-arrestins (3, 5, 10–12). Present in all eukaryotes except for plants, α-arrestins share the ability to perform desensitization (13, 14). Beyond desensitization, non-traditional arrestin roles have been recently elucidated in model fungi. Fungal α-arrestins often act as scaffolds, physically bringing different components of signaling cascades within functional proximity of each other (10, 15–17). Additionally, other fungal α-arrestins function as adaptors, facilitating proper localization

and function of other proteins. They often serve as ubiquitin ligase adaptors by means of proline-rich ubiquitin ligase binding motifs, or PxY sites, but α-arrestins can also act as adaptors for cytosolic proteins beyond those involved in ubiquitination (14, 18–21). Through these mechanisms, arrestins enable eukaryotic cells to terminate, promote, and modulate diverse adaptive cellular response signaling pathways both at the plasma membrane and throughout the cytosol.

The regulation of adaptive cellular responses is particularly important for pathogenic fungi because, in order to cause disease, they must quickly adjust to the hostile environment of the human host. Our laboratory and others have defined many fungal adaptive cellular response pathways, such as the Ras1 pathway and the Rim alkaline pH-sensing pathway, that are required for fungal virulence (22–27). However, the mechanisms by which adaptive cellular responses are regulated in pathogenic fungi are incompletely understood. The human fungal pathogen *Cryptococcus neoformans* is able to transition from its natural reservoir in the soil to establish infection in the host, resulting in more than 180,000 infection-related deaths annually, especially among immunocompromised patients (28). In contrast to other fungal model systems that encode numerous α-arrestin proteins in their genomes, we identified four α-arrestin proteins in *C. neoformans*: Ali1, Ali2, Ali3, and Ali4. This limited set of arrestin proteins allows for investigations of individual arrestin protein function, as well as assessment of arrestins as a collective family. Using Ali1 as a model, we report that Ali1 is a novel regulator of cytokinesis, and that this regulatory role is particularly important in the presence of stress. Additionally, we determine that Ali1 regulates cytokinesis through a typical arrestin role, likely functioning as an adaptor protein. Lastly, we demonstrate

that, although Ali1 is not individually required for fatal infection, the α-arrestin family as a whole contributes to fungal virulence. By using the *C. neoformans* α-arrestins to explore the mechanisms by which fungal pathogens regulate their adaptive cellular responses, we can gain a deeper understanding of the establishment and progression of fungal infections.

RESULTS

C. neoformans contains a small family of four arrestin proteins.

Previous work recently reported two putative α-arrestin proteins in the *C. neoformans* proteome, Ali1 (CNAG_02857) and Ali2 (CNAG_02341) (Arrestin-Like 1 and 2) (Fig. 1) (25). These proteins were identified as α-arrestins based on the presence of the N-terminal and C-terminal arrestin domains. We performed a search of the *C. neoformans* proteome to identify all α-arrestin domain-containing proteins (29). In doing so, we identified two additional α-arrestin proteins, Ali3 (CNAG_ 04137) and Ali4 (CNAG_ 05343), each of which contains a single C-terminal arrestin domain (Fig. 1). In addition to the arrestin domains, each of the identified *C. neoformans* α-arrestin proteins also contains multiple ubiquitin ligase binding sites, or PxY sites, which are common features of α-arrestins (Fig. 1) (3, 12, 14). For the sake of simplicity, the *C. neoformans* α-arrestins will simply be referred to as “arrestins” throughout the remainder of this manuscript.

To prioritize our studies, we compared the protein sequence of each of the *C. neoformans* arrestin proteins with those in *Saccharomyces cerevisiae* and humans, two organisms with well-characterized arrestin families. Because there is often limited protein sequence conservation between arrestins in different species, we used two different programs within the Basic Local Alignment Search Tool (BLAST) algorithm. Protein-protein BLAST (blastp) was utilized to detect arrestin proteins in the *S. cerevisiae* and human proteomes with moderate to high degrees of homology with the *C. neoformans* arrestin proteins (30). We also used Position-Specific Iterated BLAST (PSI-BLAST) to detect arrestin proteins in the *S. cerevisiae* and human proteomes with

low, but potentially relevant, degrees of homology with the *C. neoformans* arrestin proteins (31, 32). Ali1 was the only *C. neoformans* arrestin protein that shared significant sequence homology with multiple *S. cerevisiae* arrestins and a human arrestin (Tables S1 & S2). In all of these instances, the identified sequence homology was located within the arrestin domains of both proteins. We therefore elected to focus our initial studies on Ali1.

Ali1 exhibits cell cycle-regulated localization that is dependent on the Ras signaling pathway.

We first investigated the subcellular localization of Ali1, positing that its localization would be indicative of function. We C-terminally tagged Ali1 with green fluorescent protein (GFP) and validated proper expression, stability, and function of the Ali1-GFP fusion protein using quantitative real time PCR, western blotting, and mutant phenotype complementation, respectively (data not shown). Following validation, we incubated the wild-type (WT) strain and the Ali1-GFP strain to mid-logarithmic growth phase in yeast-peptone-dextrose (YPD) medium at 30°C, a nutrient-rich growth condition, and tissue culture (TC) medium at 37°C, a stressful condition that more closely mimics the host environment. Using epifluorescence microscopy, we observed identical patterns of localization in both conditions: Ali1-GFP localizes diffusely throughout the cytoplasm and is excluded from the vacuole in non-budding cells (Fig. 2A). However, in budding cells, Ali1-GFP is enriched at the developing septum, and it also localizes within discrete puncta at the poles (Fig. 2A). To confirm this localization, we performed subcellular fractionations to measure the relative abundances of Ali1-GFP within the soluble (cytoplasmic) and insoluble (membrane-associated) cellular

fractions. We observed that Ali1-GFP is enriched in the insoluble fraction, indicating that Ali1-GFP is associated with insoluble cellular components such as the plasma membrane, intracellular membranes, and cell wall components (Fig. 2B). Together these observations suggest that Ali1 may be a novel contributor to cell polarity and/or cell division.

Previous work in our group identified *C. neoformans* Ras1 as a GTPase that is required for cytokinesis and polarized growth, particularly in the presence of cell stress (22, 23, 33). Therefore, we hypothesized that Ras1 might also be required for the cell cycle-associated localization of Ali1-GFP. To test this, we constructed a strain that, in addition to expressing *ALI1-GFP*, also expressed *mCherry-RAS1* under a galactose-regulatable promoter (23). When incubated in galactose as the sole carbon source (YPGal), cells express *RAS1* at levels similar to WT cells, which is confirmed by mCherry-Ras1 localization to the plasma membrane. In contrast, *RAS1* expression is repressed when this strain is incubated in glucose as the sole carbon source (YPD). When incubated in YPGal (WT) conditions, Ali1-GFP localizes to the septum and poles of dividing cells as previously observed (Fig. 2C). However, in YPD (*ras1*Δ) conditions, Ali1-GFP localization to the septum and poles of budding cells is impaired (Fig. 2C). We quantified the frequency of Ali1-GFP localization to the septum and poles specifically among budding cells and observed that the polarized pattern of Ali1-GFP localization is significantly decreased in YPD (*ras1*Δ) conditions compared to YPGal (WT) conditions (Fig. 2D). These data indicate that Ali1-GFP localization to sites associated with cell polarity is dependent on Ras1.

Ali1 is a regulator of cytokinesis.

From the distinct, cell cycle-regulated localization pattern of Ali1-GFP, we hypothesized that Ali1 is involved in the process of cell division. To test this hypothesis, we constructed a loss-of-function *ali1*Δ mutant and analyzed this strain for cytokinesis defects. *C. neoformans* cells with loss-of-function mutations in septin genes, known contributors to cytokinesis, exhibit cytokinesis defects when grown at elevated temperatures (34). We incubated the WT strain, the *ali1*Δ mutant, and the complemented (*ali1*Δ + *ALI1*) strain at the permissive temperature of 30°C, or the more stressful temperature of 39°C, and assessed the cells for cytokinesis defects by DIC microscopy. We observed that the *ali1*Δ mutant exhibits similar morphology to the WT strain at 30°C (Fig. 3A). However, at 39°C, we observed that the *ali1*Δ mutant displays an increased incidence of cytokinesis defects, specifically elongated cells, wide bud necks, and cells that fail to complete cytokinesis (Fig. 3A) (23, 34). We quantified this observation and found that the *ali1*Δ mutant exhibits a higher frequency of cytokinesis defects at 39°C than the WT strain, and that this *ali1*Δ mutant phenotype is rescued by complementation with the WT *ALI1* allele (Fig. 3B & S1). This observation implicates Ali1 in the regulation of cytokinesis.

Because the temperature-dependent cytokinesis phenotype of the *ali1*Δ mutant mimics that of septin mutants, we next hypothesized that Ali1 is required for septin protein complex formation. To do so, we analyzed septin protein localization in the WT strain compared to the *ali1*Δ mutant. Using epifluorescence microscopy, we observed that the septin protein, Cdc10-mCherry, localizes to the septum of budding cells in both the WT and *ali1*Δ mutant backgrounds, indicating that Ali1 is not required for assembly of septin proteins at the site of septum formation (Fig. 3C). Although Ali1 is not required

for this particular septin protein localization, we next hypothesized that Ali1 may be involved in cytokinesis by modulating the function of other interacting proteins at the septum and poles.

Ali1-GFP interacts with proteins involved in lipid metabolism.

To better understand the mechanism by which Ali1 regulates cytokinesis, we performed a proteomic screen to identify potential protein interactors of Ali1. To do so, we incubated the Ali1-GFP strain, and the WT strain as a negative control, to mid-logarithmic growth phase in YPD medium. We subsequently conditioned the cultures in YPD or TC media at 30°C, in order to capture protein-protein interactions at the most permissive temperature, for three hours. Following cell lysis, GFP immunoprecipitations were performed to enrich for Ali1-GFP. The immunoprecipitations were then analyzed by LC/ESI/MS/MS to identify proteins that potentially interact with Ali1-GFP in these two conditions. A total of 1,122 proteins were identified as potential Ali1-GFP interactors using this approach (Table S3). We applied unbiased methods to enrich for proteins in both YPD and TC conditions that were highly represented in the Ali1-GFP immunoprecipitations and lowly represented, if at all, in the respective WT immunoprecipitation. This prioritization scheme resulted in 59 and 62 potentially biologically-relevant protein interactors of Ali1-GFP in YPD and TC conditions, respectively (Tables S4 & S5). Table 1 displays the top 30 hits from this experiment in YPD medium, organized by decreasing average exclusive unique peptide count (APC) and increasing APC indentified in the WT immunoprecipitation. Table 2 displays the top 30 hits from this experiment in TC medium, organized by decreasing APC and increasing APC indentified in the WT immunoprecipitation.

We observed that the Ali1-GFP protein interactome, both in YPD and TC conditions, was enriched in proteins involved in two biological processes: protein localization/stability and lipid metabolism. Enrichment of proteins involved in protein localization/stability, such as ubiquitination proteins, has been reported for arrestins in other organisms, particularly arrestins that perform adaptor functions (1, 11, 12, 35). Ubiquitination proteins were found in both conditions, but were more highly represented in TC conditions along with various proteasome subunits (Tables 1 & 2; Tables S4 & S5). Supporting our Ali1-GFP localization observations, the septin proteins Cdc10, Cdc11, and Cdc12 were also identified at low abundances, indicating potential transient interactions with Ali1-GFP (Table S3). Interestingly, in addition to protein localization/stability, the interactome of Ali1-GFP was highly enriched in proteins involved in lipid metabolism. Multiple proteins involved in lipid synthesis and degradation were identified in both YPD and TC conditions. Specifically, the fatty acid synthase β subunit, Fas1, was the overall strongest potential interactor in both conditions (Tables 1 & 2). The enzymatic partner of Fas1, the fatty acid synthase α subunit, Fas2, was also identified at very high abundances in both YPD and TC conditions (Tables 1 & 2). The observation that Fas1 and Fas2 were the most abundant interactors in multiple, independent experiments conducted in both YPD and TC conditions, as well as the fact that previous proteomic experiments we have conducted with other proteins of interest did not find enrichment of the fatty acid synthases, suggest that Fas1 and Fas2 are true, specific interactors of Ali1 (26). These data indicate that Ali1 may be involved in the regulation of localized lipid production at the

245 developing septum and poles of budding cells, assisting in efficient cytokinesis,
246 especially in stressful growth conditions.

247 **The *ali1*Δ mutant has impaired cell surface integrity that is rescued by lipid**
248 **precursor supplementation.**

249 Using the data collected from the Ali1-GFP proteomic screen, we further
250 explored the mechanism by which Ali1 regulates cytokinesis. As previously discussed,
251 we identified many potential interactors of Ali1-GFP involved in lipid metabolism, a
252 process that is essential for proper synthesis and organization of the cell surface,
253 specifically the cell membrane. Therefore, we assessed the cell surface integrity of the
254 *ali1*Δ mutant. We incubated the WT strain, the *ali1*Δ mutant, and the *ali1*Δ + *ALI1* strain
255 at 30°C in the presence of various cell surface stressors: calcofluor white, Congo red,
256 SDS, and caffeine (36–39). The *ali1*Δ mutant exhibits modest susceptibility to caffeine,
257 a cell surface stressor that serves as a marker of cell surface integrity, when incubated
258 at 30°C (Fig. 4A) (40, 41). This phenotype is drastically enhanced when the *ali1*Δ
259 mutant is incubated at the more stressful temperature of 37°C (Fig. 4B). At both
260 temperatures, this sensitivity is rescued by complementation with the WT *ALI1* allele,
261 indicating likely alterations to the *ali1*Δ mutant cell surface.

262 As well as its role as a cell surface stressor, caffeine is an inhibitor of the target
263 of rapamycin complex 1 (TORC1) (36, 40). To determine if Ali1 functions in a pathway
264 related to TORC1 function, we assessed the sensitivity of the *ali1*Δ mutant strain to
265 rapamycin. We observed a two-fold decrease in the rapamycin MIC for the *ali1*Δ mutant
266 compared to the WT strain at both 30°C (*ali1*Δ MIC_{50} = 1.56 ng/mL; WT MIC_{50} = 3.12
267 ng/mL) and 37°C (*ali1*Δ MIC_{50} = 0.78 ng/mL; WT MIC_{50} = 1.56 ng/mL). Inhibition of

TORC1 induces autophagy in yeast (42). If caffeine-mediated inhibition of TORC1 is more effective in the *ali1*Δ mutant than in the WT strain, causing the *ali1*Δ mutant to display caffeine sensitivity, the *ali1*Δ mutant should be more susceptible to inducers of autophagy than the WT strain. Given the minimal change in rapamycin sensitivity of the *ali1*Δ mutant, we assessed the ability of the *ali1*Δ mutant strain to survive in nitrogen deprivation, a known inducer of autophagy (43). We incubated the WT strain, the *ali1*Δ mutant strain, and the *ali1*Δ + *ALI1* strain on synthetic low-ammonium dextrose (SLAD) medium at 30°C and 37°C. We observed that all strains displayed similar growth kinetics (data not shown). These data suggest that the caffeine sensitivity of the *ali1*Δ mutant is not due to dysregulation of autophagy, and that Ali1 likely does not directly function in a TORC1-related pathway.

In addition to the observation that the two strongest potential interactors of Ali1-GFP were Fas1 and Fas2, we also found that the fatty acid synthase inhibitor, cerulenin, is slightly more active against the *ali1*Δ mutant (MIC_{50} = 0.15 μg/mL) than the WT strain (MIC_{50} = 0.3 μg/mL). From these data, we hypothesized that the caffeine susceptibility of the *ali1*Δ mutant may be caused by impaired lipid synthesis. We supplemented the caffeine medium with various compounds involved in lipid synthesis and utilization, media additions that are frequently used to support the *in vitro* growth of lipid auxotrophic fungi such as *Malassezia* species (44). The addition of ox bile (10 mg/mL), which aids in the degradation and absorption of lipids, and Tween 60 (1%), which serves as an emulsifier, rescued the caffeine sensitivity of the *ali1*Δ mutant at 30°C, but not at 37°C (Fig. 4). The addition of glycerol (0.4%), a precursor for phospholipids and triglycerides, completely rescued the caffeine sensitivity of the *ali1*Δ

mutant at both 30°C and 37°C (Fig. 4). In order to eliminate the possibility that glycerol was solely providing osmotic support that allowed for the *ali1*Δ mutant to overcome its caffeine sensitivity, we also supplemented the caffeine medium with sorbitol (1 M) and observed that it did not rescue the caffeine sensitivity of the *ali1*Δ mutant at either temperature (data not shown) (45, 46). Collectively, these observations indicate that lipid precursor supplementation is sufficient to suppress the caffeine sensitivity of the *ali1*Δ mutant, suggesting that the loss of cell surface integrity of the *ali1*Δ mutant is caused in part by impaired localized lipid synthesis and/or deposition, potentially at the site of cell separation.

The *C. neoformans* arrestin family supports virulence *in vitro* and *in vivo*.

Because we observed that the *ali1*Δ mutant exhibits phenotypes that are relevant to pathogenesis, specifically cytokinesis defects at elevated temperature and sensitivity to the cell surface stressor caffeine, we hypothesized that Ali1 may support fungal virulence. As a preliminary assessment, we evaluated the ability of the *ali1*Δ mutant to survive and proliferate in an *in vitro* macrophage co-culture system (26, 47, 48). We co-cultured the WT strain, the *ali1*Δ mutant, and the *ali1*Δ + *ALI1* strain for 24 hours with J774A.1 murine macrophages. We observed that the *ali1*Δ mutant displays a moderate, reproducible reduction in its ability to survive in the presence of macrophages compared to the WT strain, a phenotype that is rescued by complementation with the WT *ALI1* allele (Fig. 5A). We then performed *in vivo* studies in a murine inhalation model of cryptococcal infection (38, 48, 49). Following intranasal inoculation of C57BL/6 mice (n = 10) with 10^4 colony forming units (CFU) of each strain, we observed no differences between the WT strain and the *ali1*Δ mutant in their abilities to cause lethal infection

(Fig. 5B). From these results, we concluded that Ali1 has modest contributions to *in vitro* survival in the presence of macrophages, but does not promote *in vivo* virulence in a murine inhalation infection model.

Because the *ali1*Δ mutant individually does not exhibit significant virulence defects, we next determined whether the *C. neoformans* arrestin family, collectively, contributes to virulence. To do so, we utilized the *ali1*Δ*ali2*Δ*ali3*Δ*ali4*Δ mutants, referred to as the "arrestin null" mutants, in which all four known *C. neoformans* arrestins are ablated. Similar to our studies with the *ali1*Δ mutant, we evaluated the ability of three independent arrestin null mutants to survive and proliferate in an *in vitro* macrophage co-culture system (26, 47, 48). To do so, we co-cultured the WT strain, the *MAT*a KN99 strain (which was used in genetic crosses to generate the arrestin null mutants), and three arrestin null mutants for 24 hours with J774A.1 murine macrophages. We observed that all three arrestin null mutants exhibit a marked reduction in their abilities to survive in the presence of macrophages, compared to the WT strain and the *MAT*a KN99 strain (Fig. 5C). A representative arrestin null mutant, *ali1*Δ*ali2*Δ*ali3*Δ*ali4*Δ - #2 (CLT57), was then assessed for virulence in the murine inhalation model (38, 48, 49). Following intranasal inoculation of C57BL/6 mice (n = 10) with 10^4 CFU of the WT strain or the arrestin null mutant, we observed that the arrestin null mutant displays a significant attenuation in virulence compared to the WT strain (Fig. 5D). Mice infected with the WT strain exhibited a median survival time of 28 days, while those infected with the arrestin null mutant exhibited a median survival time of 45.5 days (Fig. 5D). These data collectively indicate that the *C. neoformans* arrestin family contributes to both *in vitro* and *in vivo* virulence.

The *C. neoformans* arrestins likely serve distinct cellular functions.

In order to identify possible mechanisms by which the *C. neoformans* arrestin family contributes to virulence, we created individual *ali1*Δ, *ali2*Δ, *ali3*Δ, and *ali4*Δ loss-of-function mutants. Following strain confirmation, we assessed the growth kinetics of the arrestin mutants in the presence of various cellular stressors. Specifically, we incubated the WT strain, the individual arrestin mutants, and the arrestin null mutants in the presence of physiologically-relevant stressors, such as elevated temperature (39°C), high salt (1.5 M NaCl), and alkaline pH (pH 8), as well as cell surface stressors, such as caffeine (1 mg/mL) and SDS (0.03%) (25, 39, 40, 50). We observed that the individual arrestin mutants display distinct, but overlapping, phenotypes in the presence of these stressors (Fig. 6). All of these individual arrestin mutant phenotypes are rescued by complementation with the respective WT arrestin allele (Fig. S2).

Because we observed that the *ali2*Δ mutant has an enhanced caffeine sensitivity phenotype compared to the *ali1*Δ mutant, we hypothesized that the *ali2*Δ mutant would display more severe virulence defects than the *ali1*Δ mutant. To test this hypothesis, we co-cultured the WT strain, the *ali2*Δ mutant, the *ali2*Δ + *ALI2-GFP* strain, and an *ali1*Δ*ali2*Δ mutant for 24 hours with J774A.1 murine macrophages. The *ali2*Δ mutant had a significant reduction in its ability to survive in the presence of macrophages compared to the WT strain, a phenotype that is rescued by complementation with the WT *ALI2* allele (Fig. S3). The *ali2*Δ mutant survival rate (67%) is lower than what was observed for the *ali1*Δ mutant (79%) (Fig. 5A). Additionally, the *ali1*Δ*ali2*Δ mutant exhibits a more severe survival impairment (43%) than either the *ali1*Δ mutant or *ali2*Δ mutant alone,

359 indicating that Ali1 and Ali2 have additive effects that contribute to survival in the
360 presence of macrophages.

361 The arrestin null mutants share many phenotypes with the individual arrestin
362 mutants, such as sensitivity to high temperature, caffeine, and high salt, as well as
363 resistance to SDS (Fig. 6). Uniquely, the arrestin null mutants display a slight increase
364 in growth rate in the presence of alkaline pH (Fig. 6). The most pronounced phenotypes
365 of the arrestin null mutants, growth defects in the presence of high temperature and
366 caffeine, were not rescued by glycerol (0.4%) supplementation but were partially
367 rescued by osmotic support with sorbitol (1M) supplementation (Fig. S4). These data
368 suggest that the *C. neoformans* arrestin proteins likely perform distinct, nonredundant
369 cellular functions that contribute to survival in physiologically-relevant conditions and
370 cell surface stability.

DISCUSSION

Arrestins have been well-characterized in model fungi systems.

The model ascomycete fungi, such as *S. cerevisiae*, *Aspergillus nidulans*, and *Schizosaccharomyces pombe*, all contain relatively large α-arrestin families of nine to eleven members (29). Based on the presence of the conserved arrestin domains, α-arrestins are predicted to exist in the other three major fungal groups: the basidiomycetes, the zygomycetes, and the chytrids (29). We used *C. neoformans* as a genetically-tractable basidiomycete, with a relatively small arrestin family of four members, to more broadly characterize fungal α-arrestin functions, both individually and collectively. Additionally, because *C. neoformans* is a major human pathogen, we interrogated the functional contributions of fungal α-arrestins to virulence. The fact that the α-arrestins, despite lacking catalytic activity themselves, have remained present within all major fungal groups indicates that they are likely functionally important proteins within the fungal kingdom.

Ali1 is important for cytokinesis in the presence of cellular stress.

Septins are conserved GTP-binding proteins that create the septum in eukaryotes, often serving as scaffolds for other proteins that direct cell cycle progression (51–53). In *S. cerevisiae*, the septin proteins assemble into filaments at the mother bud neck, creating the hourglass-shaped septum, and are required for normal cytokinesis (53). The *C. neoformans* septins have been shown to function similarly. *C. neoformans* septin mutants display cytokinesis defects when incubated at elevated temperatures and also display modest sensitivity to cell surface stressors, such as caffeine and SDS (34).

We observed that Ali1 has cell cycle-associated localization, with enrichment at the septum and poles of budding cells. Our protein interactome analysis supported this observation, with multiple septin proteins, Cdc10, Cdc11, and Cdc12, identified at low levels in the Ali1-GFP immunoprecipitations. Protein-protein interactions with septin proteins are typically transient, potentially explaining the low APC for the septin proteins using this experimental approach (54). Additionally, we found that the *ali1*Δ mutant displays an increased incidence of cytokinesis defects at elevated temperature and sensitivity to the cell surface stressor caffeine, thus phenocopying the *C. neoformans* septin mutants (34). These data suggest that Ali1 is a regulator of cytokinesis that is particularly important in the presence of stress. Whole transcriptome analyses of synchronized *C. neoformans* cells have shown that Ali1 expression is cyclic, or regulated with the cell cycle, with its peak expression occuring about 15 minutes prior to bud emergence (55). As a potential regulator of cytokinesis, this expression pattern would enable the *ALI1* transcript to be transcribed, and the Ali1 protein to be translated and localize to the septum and poles as cell division is occuring.

In addition to and in collaboration with septins, Ras GTPases are conserved regulators of cell division in eukaryotes. Our laboratory has shown that the *C. neoformans* Ras1 protein directs polarized growth and actin polarization, particular in the presence of stress (22, 23, 33). When Ras1 is inhibited, septins are unable to organize at the septum to perform their scaffolding functions and cells display morphological and cytokinesis defects (23). We demonstrated that in the absence of Ras1, Ali1 localization to the septum and poles is impaired. This observation indicates that the cell cycle-regulated localization of Ali1 is dependent on Ras1.

Ali1 likely fulfills an adaptor role aiding cytokinesis.

Cytokinesis is a highly organized and regulated process in fungi. In *S. cerevisiae*, cell wall enzymes, such as the β(1-3)-glucan synthases and the chitin synthases, localize to the septum and poles to help build the septum and cell wall during cell division. (56–58). It is believed that *C. neoformans* also directs cytokinesis similarly. For example, *C. neoformans* cells lacking Chs3, a chitin synthase, or Ags1, the α(1-3)-glucan synthase, display cytokinesis defects during budding (59, 60). Similar to the cell wall, the cell membrane must be remodeled to aid in bud growth and cytokinesis in fungi. To our knowledge, little work has focused on the degradation and rebuilding of the fungal cell membrane during cytokinesis. However, in the bacterium *Mycobacterium tuberculosis*, fatty acid synthase proteins localize to the poles and septum to synthesize the mycomembrane during cell division (61).

Fungal fatty acid synthases, which belong to the microbial type I fatty acid synthase family, are cytosolic multi-enzymes that heterodimerize to form hexamers (α6β6) (62–64). Once in this complex, they employ their individual component enzymes to synthesize de novo a diversity of lipid products that are used for cellular metabolism, signaling, and biological membranes. In *C. neoformans*, Fas1 and Fas2 are required for viability in standard laboratory conditions and are targets of the fatty acid synthase inhibitor cerulenin (65). Through our protein interactome analysis, we found that the two strongest potential interactors of Ali1 are Fas1 and Fas2. We tested the sensitivity of the *ali1*Δ mutant to cerulenin and observed that the *ali1*Δ mutant strain is slightly more sensitive to cerulenin than the WT strain. In conjunction with these data, we observed that the *ali1*Δ mutant displays sensitivity to the cell surface stressor caffeine, which is

440 enhanced in the presence of temperature stress. In addition to its roles as a cell surface
441 stressor, caffeine is believed to inhibit TORC1 (36, 40). The caffeine sensitivity of the
442 *ali1*Δ mutant may be explained by the fact that TORC1 is an upstream activator of lipid
443 synthesis genes in eukaryotes, including fatty acid synthases (66–68). Supplementation
444 with exogenous lipid precursors, but not the osmotic stabilizer sorbitol, may reverse the
445 caffeine sensitivity of the *ali1*Δ mutant by compensating for an insufficiency in
446 substrates used to synthesize cellular membranes. These data collectively suggest that
447 Ali1 is required for complete Fas1 and Fas2 function.

448 The *S. pombe* α-arrestin, Art1, regulates cytokinesis through its adaptor function
449 (69). Art1 is required for the localization of Rgf3, the guanine nucleotide exchange factor
450 for the regulatory subunit of the β-glucan synthase, Rho1, to the septum, likely so that it
451 can help build the septum. Our data suggest that Ali1 functions similarly to Art1. We
452 hypothesize that Ali1 acts as an adaptor for Fas1 and Fas2, aiding in their localization to
453 the septum and poles, so that they can rebuild the cell membrane during cytokinesis
454 (Fig. 7). In the absence of Ali1, cells are left with small, localized defects in the cell
455 surface because they are unable to repair the membrane, or are delayed in membrane
456 repair, compared to WT cells, particularly in the presence of stress. This results in the
457 cytokinesis and cell surface defects observed in the *ali1*Δ mutant. Previous work in both
458 mammals and fungi have demonstrated the importance of fatty acid synthesis for
459 progression through the cell cycle (70–72). Additionally, the mechanism by which Ali1 is
460 able to perform its adaptor function for Fas1 and Fas2 may be ubiquitin-mediated,
461 through interactions with the E3 ubiquitin ligase Rsp5 (Fig. 7). Ali1 contains four
462 potential ubiquitin ligase binding sites, or PxY sites. We also observed that Ali1 interacts

463 with multiple ubiquitination proteins, including E1, E2, and E3 proteins, particularly in TC
464 conditions (73). Ubiquitination is most often considered in the context of proteasomal
465 degradation, but it can also direct diverse subcellular localizations (74–76).
466 Future investigations can explore the interactions between Ali1 and the fatty acid
467 synthases, Fas1 and Fas2. Additionally, the localizations of Fas1 and Fas2 in the WT
468 and the *ali1*Δ mutant backgrounds can also be assessed. However, it is possible that it
469 may be difficult to draw conclusions from these experiments. Fas1 and Fas2 are
470 abundant, diffusely cytosolic proteins in *S. cerevisiae* (77). If this is also the case for *C.*
471 *neoformans*, it may be challenging to observe any transient interactions or enrichments
472 of these proteins at the septum and poles.
473 **The *C. neoformans* arrestin family contributes to virulence.**
474 Upon infection, pathogens must regulate their adaptive cellular responses to
475 acclimate to the stressors of the host environment. Work largely conducted in
476 ascomycete fungi has demonstrated that disruption of α-arrestin-regulated adaptive
477 cellular responses is detrimental for fungal survival and pathogenesis. For example, the
478 α-arrestin Rim8 scaffolds the Rim alkaline pH response pathway in *Candida albicans*;
479 the *rim8*Δ mutant displays attenuation in a murine model of systemic candidiasis,
480 indicating that Rim8 is required for adaptation to the host environment (78). Given many
481 investigations demonstrating that human arrestin proteins regulate cellular processes
482 that are involved in human disease, we propose that fungal arrestins similarly regulate
483 fungal adaptive cellular responses important for disease establishment and progression
484 (79–82).

485 This study directly investigates the virulence contributions of fungal α-arrestins.
486 Implementing a murine inhalation model of cryptococcal infection, we observed that the
487 individual *ali1*Δ mutant does not display virulence attenuation, but that the arrestin null
488 mutant exhibits a significant delay in its ability to cause fatal disease. These data
489 suggest that the arrestins, collectively, are involved in adaptation to the host
490 environment in *C. neoformans*. Since we observed that the *ali2*Δ mutant displays more
491 severe attenuation in its ability to survive in the presence of macrophages than the *ali1*Δ
492 mutant, we propose that Ali2 is a compelling subject for future investigations.
493 Additionally, because the arrestin mutants have distinct phenotypes in the presence of
494 different cellular stressors, as well as because the *C. neoformans* arrestin family is very
495 small, we hypothesize that the *C. neoformans* arrestins have distinct cellular functions
496 that contribute to adaptation to the host. Functional redundancy has been observed for
497 mammalian and fungal arrestins, therefore it is possible that the *C. neoformans*
498 arrestins could have some degree of overlapping functions while maintaining protein-
499 specific activities as well (19, 83).
500 We have demonstrated that the *C. neoformans* arrestin family contains four
501 members that share little primary amino acid sequence conservation with human
502 arrestins. These fungal-specific proteins likely mediate various cellular functions
503 including efficient progression through the cell cycle, especially under stressful growth
504 conditions. Fungal arrestins therefore offer unique insight into mechanisms of stress
505 response and cellular adaptation in this diverse group of eukaryotes.

MATERIALS AND METHODS

Strains, media, and growth conditions

All strains used in this study were generated in the *C. neoformans* var. *grubii* H99 (*MAT*α) or KN99 (*MAT*a) backgrounds and are included in Table 3. Strains were maintained on yeast extract-peptone-dextrose (YPD) medium (1% yeast extract, 2% peptone, 2% dextrose, and 2% agar for solid medium). To regulate *RAS1* expression, yeast extract-peptone-galactose (YPGal) medium (1% yeast extract, 2% peptone, and 3% galactose) was utilized (23). CO_2-independent tissue culture (TC, Gibco) medium was used to mimic an *in vivo* environment, as described previously (84). To assess mutant strain cell surface phenotypes, NaCl (1.5 M) and Congo red (0.5%) were added to YPD medium before autoclaving, while caffeine (1 mg/mL), calcofluor white (1 mg/mL), and SDS (0.03%) were filter sterilized and added to YPD medium after autoclaving (38). Synthetic low-ammonium dextrose (SLAD) medium (0.17% yeast nitrogen base without amino acids and without ammonium sulfate, 50 μM ammonium sulfate, 2% dextrose, and 2% agar) was used as a nitrogen deprivation medium to induce autophagy. Lipid precursor supplementation was achieved by adding ox bile (HiMedia Labs) (10 mg/mL) and Tween 60 (1%) to medium before autoclaving, or by adding sterile glycerol (0.4%) to medium after autoclaving. Sorbitol supplementation was achieved by adding sorbitol (1M) to medium before autoclaving. Alkaline pH plates were made by adding 150 mM HEPES buffer to YPD medium and adjusting the pH to 8.15 with NaOH prior to autoclaving (25). Unless otherwise indicated, strains were incubated at 30°C.

Molecular biology and strain construction

All plasmids used in this study are listed in Table 4. All primers utilized in this study are listed in Table 5. All strains were generated by biolistic transformation, unless otherwise described (85). Detailed methods for the construction of all strains used in this study are included in File S1 (86–88).

BLAST analyses

To identify homology between the *C. neoformans* arrestins and those in *S. cerevisiae* and humans, Basic Local Alignment Search Tool (BLAST, NCBI) was used. The protein sequences of each of the *C. neoformans* arrestins was searched against the *S. cerevisiae* S288C (taxid:559292) and human (taxid:9606) proteomes using the default parameters for protein-protein BLAST (blastp) and Position-Specific Iterated BLAST (PSI-BLAST) (30–32). Alignments considered significant, those with E values less than 1, are included in Tables S1 (*S. cerevisiae*) and S2 (human).

Fluorescent and light microscopy

All images in this study (differential interference contrast [DIC] and fluorescent) were captured using a Zeiss Axio Imager A1 microscope equipped with an Axio-Cam MRM digital camera. To assess subcellular localization of Ali1-GFP, the WT (H99) strain and the Ali1-GFP (CLT7) strain were incubated for 18 hours with 150 rpm shaking in YPD medium at 30°C or TC medium at 37°C. Cells were then pelleted, washed with phosphate-buffered saline (PBS), and imaged.

To measure the frequency of cell cycle-associated localization of Ali1-GFP in the presence and absence of Ras1, the Ali1-GFP + mCherry-Ras1 (CBN486) strain was incubated for 18 hours at 30°C with 150 rpm shaking in YPGal medium. Cells were pelleted, washed three times with PBS, normalized by spectrophotometry, and then

552 resuspended to an OD_{600} of 0.2 in either YPGal medium (to induce *RAS1* expression) or
553 YPD medium (to repress *RAS1* expression) for 18 hours at 30°C with 150 rpm shaking
554 (23). Cells were then pelleted, washed with PBS, and imaged. Results are reported as
555 the average percentage (+/- standard error of the mean [SEM]) of actively budding cells
556 that displayed Ali1-GFP localization to the septum and/or poles. Statistical significance
557 was determined using Student's *t*-test (GraphPad Software, San Diego, CA). A
558 minimum of 600 cells were analyzed in both YPGal and YPD conditions across three
559 biological replicates using ImageJ Software (Fiji) (89, 90).

560 To analyze the morphology of the *ali1*Δ mutant cells, the WT (H99), *ali1*Δ
561 (KS120), and *ali1*Δ + *ALI1* (CLT6) strains were incubated for 18 hours at 30°C with 150
562 rpm shaking in YPD medium. An OD of approximately 0.2 for each strain was
563 transferred to fresh YPD medium and subsequently incubated at either 30°C or 39°C for
564 18 hours with 150 rpm shaking. Cells were then pelleted, washed with PBS, and
565 imaged. Results are reported as the average percentage (+/- SEM) of total cells
566 displaying morphological defects. Statistical significance was determined using one-way
567 analysis of variance (ANOVA) and the Tukey-Kramer test (GraphPad Software, San
568 Diego, CA). A minimum of 600 cells were analyzed across three biological replicates
569 using ImageJ Software (Fiji) (89, 90).

570 To assess whether Ali1 is required for septin protein localization, the Cdc10-
571 mCherry (LK001) strain and the Cdc10-mCherry + *ali1*Δ (CLT42) strain were incubated
572 for 18 hours at either 30°C or 37°C with 150 rpm shaking in YPD medium. Cells were
573 then pelleted, washed with PBS, and imaged.

574 **Protein isolation, membrane fractionation, and western blotting**

For all protein experiments, protein extracts were prepared as previously described (25, 26). Briefly, the WT (H99) and the Ali1-GFP (CLT7) strains were incubated for 18 hours at 30°C with 150 rpm shaking in YPD medium. Cells were pelleted, flash frozen on dry ice, and lysed by bead beating. The crude lysate was cleared by centrifugation at 2,500 x g at 4°C for 5 minutes and the supernatant (total cell lysate) was transferred to a new tube. Total cell lysate protein concentrations were measured using bicinchoninic acid assay (BCA).

To determine the relative abundance of Ali1 in different cellular fractions, WT (H99) and the Ali1-GFP (CLT7) strains were incubated and lysed as above. Total cell lysates (T) were separated by ultracentrifugation at 30,000 x g for 1 hour at 4°C (27). The soluble fraction (S) was transferred to a new tube and the insoluble pellet (I) was resuspended in an equivalent volume of lysis buffer containing 1% Triton X-100. All samples were normalized by total protein concentration. Western blots were performed as described previously using an anti-GFP primary antibody (1/5,000 dilution, Roche) followed by an anti-mouse peroxidase-conjugated secondary antibody (1/25,000 dilution, Jackson Labs). Proteins were detected by enhanced chemiluminescence (ECL Prime Western blotting detection reagent, GE Healthcare).

Proteomic experiment preparation and analysis

Proteomic analysis was performed with a single replicate for the WT (H99) strain in both YPD and TC conditions, and in triplicate for the Ali1-GFP (CLT7) strain in both YPD and TC conditions. To prepare total cell lysates for this experiment, the WT (H99) strain and the Ali1-GFP (CLT7) strain were incubated for 18 hours at 30°C with 150 rpm shaking in YPD medium. Both strains were normalized to an OD_{600} of 1, resuspended in

598 either YPD or TC media, and then incubated for 3 hours at 30°C with 150 rpm. Cells
599 were pelleted and lysed as described above to extract total cell lysates.
600 Immunoprecipitations from total cell lysates were performed by addition of 25 µL GFP-
601 Trap resin (Chromotek) and inversion at 4˚C for 2 hrs. Mass spectrometry analysis was
602 performed on immunoprecipitations by the Duke Proteomics Core Facility, as described
603 previously (26). A description of this analysis is included in File S1.
604 We prioritized hits from this proteomic analysis to enrich for proteins with
605 stronger potential interactions with Ali1-GFP. First, we averaged the exclusive unique
606 peptide counts (APC) for each potential interactor identified in YPD or TC conditions,
607 and subsequently selected those that had an APC of 2 or more for further analysis. We
608 then calculated the percentage of the APC that was identified in the respective WT
609 immunoprecipitation for each potential protein interactor. Those proteins that had less
610 than 20% of the APC identified in the respective WT immunoprecipitation were
611 determined to be unique interactors of Ali1-GFP. All proteins identified using this
612 prioritization scheme in YPD and TC conditions can be found in Tables S4 and S5,
613 respectively. All 1,122 identified proteins, except for those not belonging to *C.*
614 *neoformans*, are included in Table S3.
615 **Macrophage co-culture experiments**
616 The ability of strains to survive in the presence of macrophages was assessed as
617 previously described (26). Briefly, 10^5 J774.1 macrophages were incubated with 10^5
618 opsonized fungal cells – WT (H99), KN99a, *ali1*Δ (KS120), *ali1*Δ + *ALI1* (CLT6), *ali2*Δ
619 (KS96-2), *ali2*Δ + *ALI2-GFP* (CLT67), *ali1*Δ*ali2*Δ (KS97-2), and the arrestin null (CLT56,
620 CLT57, and CLT58) mutants. Co-cultures of J774.1 macrophages and phagocytosed

621 fungal cells were incubated for 24 hours at 37°C with 5% CO_2. Phagocytosed fungal
622 cells were collected, serially diluted, and plated onto YPD agar to assess the number of
623 viable *C. neoformans* cells by quantitative culture. Results are reported as the average
624 percentage (+/- SEM) of recovered colony-forming units (CFU), normalized to the WT
625 (H99) strain, generated from at least 4 biological replicates. Statistical significance was
626 determined using one-way analysis of variance (ANOVA) and the Tukey-Kramer test
627 (GraphPad Software, San Diego, CA).

628 **Mouse survival experiments**

629 The murine inhalation model of cryptococcosis was used to assess virulence of
630 the stains in this study (49). C57BL/6 female mice were acquired from Charles Rivers
631 Laboratories. Mice were anesthetized with 2% isoflurane utilizing a rodent anesthesia
632 device (Eagle Eye Anesthesia, Jacksonville, FL) and were infected via the intranasal
633 route with 10^4 CFU of either the WT (H99) strain, the *ali1*Δ (KS120) mutant, the *ali1*Δ +
634 *ALI1* (CLT6) strain, or an arrestin null (CLT57) mutant in 30 µl of sterile PBS. Mice (n =
635 10) were monitored twice daily and sacrificed if moribund. Survival data were
636 statistically analyzed using log-rank test (GraphPad Software, San Diego, CA). Animal
637 experiments were approved by The University of Texas at San Antonio Institutional
638 Animal Care and Use Committee (IACUC) and mice were handled according to IACUC
639 guidelines.

640 **Minimum inhibitory concentration (MIC) testing**

641 To measure strain susceptibilities to rapamycin and cerulenin, MIC testing was
642 performed using species-specific modifications to standard CLSI testing methods for

643 broth microdilution testing of antifungal susceptibility (91, 92). A detailed description of

644 this method is described in File S1.

ACKNOWLEDGEMENTS

This work was supported by NIH R01 grant AI074677 (J.A.A.). We would like to thank the Duke Proteomics Core Facility for assistance with our proteomic experiments. We would also like to acknowledge the Madhani laboratory at UCSF and NIH funding R01AI100272 for the publicly available deletion mutant collections in *C. neoformans* (Fungal Genetics Stock Center, 2015/2016 Madhani plates).

REFERENCES

1. Shenoy SK, Lefkowitz RJ. 2011. β-Arrestin-mediated receptor trafficking and signal transduction. *Trends Pharmacol Sci* **32**:521–33. doi:10.1016/j.tips.2011.05.002.

2. Patwari P, Lee RT. 2012. An expanded family of arrestins regulate metabolism. *Trends Endocrinol Metab* **23**:216-22. doi:10.1016/j.tem.2012.03.003.

3. Puca L, Brou C. 2014. α-Arrestins - New players in Notch and GPCR signaling pathways in mammals. *J Cell Sci* **127**:1359–67. doi:10.1242/jcs.142539.

4. Peterson YK, Luttrell LM. 2017. The diverse roles of arrestin scaffolds in G protein-coupled receptor signaling. *Pharmacol Rev* **69**:256–297. doi:10.1124/pr.116.013367.

5. Alvarez CE. 2008. On the origins of arrestin and rhodopsin. *BMC Evol Biol* **8**:1–13. doi:10.1186/1471-2148-8-222.

6. Aubry L, Guetta D, Klein G. 2009. The arrestin fold: Variations on a theme. *Curr Genomics* **10**:133–142. doi:10.2174/138920209787847014.

7. Kühn H, Hall SW, Wilden U. 1984. Light-induced binding of 48-kDa protein to photoreceptor membranes is highly enhanced by phosphorylation of rhodopsin. *FEBS Lett* **176**:473–478. doi:10.1016/0014-5793(84)81221-1.

8. Zuckerman R, Cheasty JE. 1986. A 48 kDa protein arrests cGMP phosphodiesterase activation in retinal rod disk membranes. *FEBS Lett* **207**:35–41. doi:10.1016/0014-5793(86)80008-4.

9. Benovic JL, Kühn H, Weyand I, Codina J, Caron MG, Lefkowitz RJ. 1987. Functional desensitization of the isolated β-adrenergic receptor by the β-

674 adrenergic receptor kinase: Potential role of an analog of the retinal protein
675 arrestin (48-kDa protein). *Proc Natl Acad Sci U S A* **84**:8879–82.
676 doi:10.1073/pnas.84.24.8879.
677 10. Li W, Mitchell AP. 1997. Proteolytic activation of Rim1p, a positive regulator of
678 yeast sporulation and invasive growth. *Genetics* **145**:63–73.
679 11. Boase NA, Kelly JM. 2004. A role for creD, a carbon catabolite repression gene
680 from Aspergillus nidulans, in ubiquitination. *Mol Microbiol* **53**:929–940.
681 doi:10.1111/j.1365-2958.2004.04172.
682 12. Lin CH, MacGurn JA, Chu T, Stefan CJ, Emr SD. 2008. Arrestin-related ubiquitin-
683 ligase adaptors regulate endocytosis and protein turnover at the cell surface. *Cell*
684 **135**:714–725. doi: 10.1016/j.cell.2008.09.025.
685 13. Alvaro CG, O'Donnell AF, Prosser DC, Augustine AA, Goldman A, Brodsky JL,
686 Cyert MS, Wendland B, Thorner J. 2014. Specific α-arrestins negatively regulate
687 Saccharomyces cerevisiae pheromone response by down-modulating the G-
688 protein-coupled receptor Ste2. *Mol Cell Biol* **34**:2660–81.
689 doi:10.1128/MCB.00230-14.
690 14. Prosser DC, Pannunzio AE, Brodsky JL, Thorner J, Wendland B, O'Donnell AF.
691 2015. α-Arrestins participate in cargo selection for both clathrin-independent and
692 clathrin-mediated endocytosis. *J Cell Sci* **128**:4220–34. doi:10.1242/jcs.175372.
693 15. Herrador A, Herranz S, Lara D, Vincent O. 2010. Recruitment of the ESCRT
694 machinery to a putative seven-transmembrane-domain receptor is mediated by an
695 arrestin-related protein. *Mol Cell Biol* **30**:897–907. doi:10.1128/MCB.00132-09.
696 16. Herranz S, Rodríguez JM, Bussink H-J, Sánchez-Ferrero JC, Arst HN, Peñalva

MA, Vincent O. 2005. Arrestin-related proteins mediate pH signaling in fungi. *Proc Natl Acad Sci U S A* **102**:12141–6. doi:10.1073/pnas.0504776102.

17. Gomez-Raja J, Davis DA. 2012. The β-arrestin-like protein Rim8 is hyperphosphorylated and complexes with Rim21 and Rim101 to promote adaptation to neutral-alkaline pH. *Eukaryot Cell* **11**:683–693.

18. Nikko E, Sullivan JA, Pelham HRB. 2008. Arrestin-like proteins mediate ubiquitination and endocytosis of the yeast metal transporter Smf1. *EMBO Rep* **9**:1216–1221. doi:10.1038/embor.2008.199.

19. Nikko E, Pelham HRB. 2009. Arrestin-mediated endocytosis of yeast plasma membrane transporters. *Traffic* **10**:1856–67. doi:10.1111/j.1600-0854.2009.00990.

20. O'Donnell AF, Apffel A, Gardner RG, Cyert MS. 2010. α-Arrestins Aly1 and Aly2 regulate intracellular trafficking in response to nutrient signaling. *Mol Biol Cell* **21**:3552–66. doi:10.1091/mbc.E10-07-0636.

21. Hervás-Aguilar A, Galindo A, Peñalva MA. 2010. Receptor-independent ambient pH signaling by ubiquitin attachment to fungal arrestin-like PalF. *J Biol Chem* **285**:18095–18102. doi:10.1074/jbc.M110.114371.

22. Nichols CB, Perfect ZH, Alspaugh JA. 2007. A Ras1-Cdc24 signal transduction pathway mediates thermotolerance in the fungal pathogen Cryptococcus neoformans. *Mol Microbiol* **63**:1118–1130. doi:10.1111/j.1365-2958.2006.05566.

23. Ballou ER, Kozubowski L, Nichols CB, Alspaugh JA. 2013. Ras1 acts through duplicated Cdc42 and Rac proteins to regulate morphogenesis and pathogenesis in the human fungal pathogen Cryptococcus neoformans. *PLoS Genet*

9:e1003687. doi:10.1371/journal.pgen.1003687.

24. O'Meara TR, Holmer SM, Selvig K, Dietrich F, Alspaugh JA. 2013. Cryptococcus neoformans Rim101 is associated with cell wall remodeling and evasion of the host immune responses. *MBio* **4**:e00522-12. doi:10.1128/mBio.00522-12.

25. Ost KS, O'Meara TR, Huda N, Esher SK, Alspaugh JA. 2015. The Cryptococcus neoformans alkaline response pathway: Identification of a novel rim pathway activator. *PLoS Genet* **11**:e1005159. doi:10.1371/journal.pgen.1005159.

26. Pianalto KM, Ost KS, Brown HE, Alspaugh JA. 2018. Characterization of additional components of the environmental pH-sensing complex in the pathogenic fungus Cryptococcus neoformans. *J Biol Chem* **293**:9995–10008. doi:10.1074/jbc.RA118.002741.

27. Brown HE, Ost KS, Esher SK, Pianalto KM, Saelens JW, Guan Z, Andrew Alspaugh J. 2018. Identifying a novel connection between the fungal plasma membrane and pH-sensing. *Mol Microbiol* **109**:474–493. doi:10.1111/mmi.13998.

28. Rajasingham R, Smith RM, Park BJ, Jarvis JN, Govender NP, Chiller TM, Denning DW, Loyse A, Boulware DR. 2017. Global burden of disease of HIV-associated cryptococcal meningitis: An updated analysis. *Lancet Infect Dis* **17**:873–881. doi:10.1016/S1473-3099(17)30243-8.

29. Stajich JE, Harris T, Brunk BP, Brestelli J, Fischer S, Harb OS, Kissinger JC, Li W, Nayak V, Pinney DF, Stoeckert CJ, Roos DS. 2012. FungiDB: An integrated functional genomics database for fungi. *Nucleic Acids Res* **40**:D675-81. doi:10.1093/nar/gkr918.

30. Altschul SF, Gish W, Miller W, Myers EW, Lipman DJ. 1990. Basic local alignment

search tool. *J Mol Biol* **215**:403–410. doi:10.1016/S0022-2836(05)80360-2.

31. Altschul S, Madden TL, Schäffer AA, Zhang J, Zhang Z, Miller W, Lipman DJ. 1997. Gapped BLAST and PSI-BLAST: A new generation of protein database search programs. *Nucleic Acids Res* **25**:3389–3402. doi:10.1093/nar/25.17.3389.

32. Schäffer AA, Aravind L, Madden TL, Shavirin S, Spouge JL, Wolf YI, Koonin E V, Altschul SF. 2001. Improving the accuracy of PSI-BLAST protein database searches with composition-based statistics and other refinements. *Nucleic Acids Res* **29**:2994–3005. doi:10.1093/nar/29.14.2994.

33. Alspaugh JA, Cavallo LM, Perfect JR, Heitman J. 2000. Ras1 regulates filamentation, mating and growth at high temperature of Cryptococcus neoformans. *Mol Microbiol* **36**:352–365. doi:10.1046/j.1365-2958.2000.01852.

34. Kozubowski L, Heitman J. 2010. Septins enforce morphogenetic events during sexual reproduction and contribute to virulence of Cryptococcus neoformans. *Mol Microbiol* **75**:658-75. doi:10.1111/j.1365-2958.2009.06983.

35. Girnita L, Shenoy SK, Sehat B, Vasilcanu R, Girnita A, Lefkowitz RJ, Larsson O. 2005. β-Arrestin is crucial for ubiquitination and down-regulation of the insulin-like growth factor-1 receptor by acting as adaptor for the Mdm2 E3 ligase. *J Biol Chem* **280**:24412–9. doi:10.1074/jbc.M501129200.

36. Lum PY, Armour CD, Stepaniants SB, Cavet G, Wolf MK, Butler JS, Hinshaw JC, Garnier P, Prestwich GD, Leonardson A, Garrett-Engele P, Rush CM, Bard M, Schimmack G, Phillips JW, Roberts CJ, Shoemaker DD. 2004. Discovering modes of action for therapeutic compounds using a genome-wide screen of yeast heterozygotes. *Cell* **116**:121–137. doi:10.1016/s0092-8674(03)01035-3.

766 37. Ram AFJ, Klis FM. 2006. Identification of fungal cell wall mutants using
767 susceptibility assays based on calcofluor white and congo red. *Nat Protoc*
768 **1**:2253–2256. doi:10.1038/nprot.2006.397.
769 38. Esher SK, Ost KS, Kohlbrenner MA, Pianalto KM, Telzrow CL, Campuzano A,
770 Nichols CB, Munro C, Wormley FL, Alspaugh JA. 2018. Defects in intracellular
771 trafficking of fungal cell wall synthases lead to aberrant host immune recognition.
772 *PLOS Pathog* **14**:e1007126. doi:10.1371/journal.ppat.1007126.
773 39. Schroeder L, Ikui AE. 2019. Tryptophan confers resistance to SDS-associated cell
774 membrane stress in Saccharomyces cerevisiae. *PLoS One* **14**:e0199484.
775 doi:10.1371/journal.pone.0199484.
776 40. Truman AW, Kim KY, Levin DE. 2009. Mechanism of Mpk1 mitogen-activated
777 protein kinase binding to the Swi4 transcription factor and its regulation by a novel
778 caffeine-induced phosphorylation. *Mol Cell Biol* **29**:6449–61.
779 doi:10.1128/MCB.00794-09.
780 41. Levin DE. 2011. Regulation of cell wall biogenesis in Saccharomyces cerevisiae:
781 The cell wall integrity signaling pathway. *Genetics* **189**:1145–75.
782 doi:10.1534/genetics.111.128264.
783 42. Noda T, Ohsumi Y. 1998. Tor, a phosphatidylinositol kinase homologue, controls
784 autophagy in yeast. *J Biol Chem* **273**:3963–6. doi:10.1074/jbc.273.7.3963.
785 43. Shpilka T, Welter E, Borovsky N, Amar N, Shimron F, Peleg Y, Elazar Z. 2015.
786 Fatty acid synthase is preferentially degraded by autophagy upon nitrogen
787 starvation in yeast. *Proc Natl Acad Sci U S A* **112**:1434–9.
788 doi: 10.1073/pnas.1409476112.

789 44. Kaneko T, Makimura K, Onozaki M, Ueda K, Yamada Y, Nishiyama Y,
790 Yamaguchi H. 2005. Vital growth factors of Malassezia species on modified
791 CHROMagar Candida. *Med Mycol* **43**:699–704.
792 doi:10.1080/13693780500130564.
793 45. Philips J, Herskowitz I. 1997. Osmotic balance regulates cell fusion during mating
794 in Saccharomyces cerevisiae. *J Cell Biol* **138**:961–74. doi:10.1083/jcb.138.5.961.
795 46. Hartland K, Pu J, Palmer M, Dandapani S, Moquist PN, Munoz B, DiDone L,
796 Schreiber SL, Krysan DJ. 2016. High-throughput screen in Cryptococcus
797 neoformans identifies a novel molecular scaffold that inhibits cell wall integrity
798 pathway signaling. *ACS Infect Dis* **2**:93–102. doi:10.1021/acsinfecdis.5b00111.
799 47. Feldmesser M, Kress Y, Novikoff P, Casadevall A. 2000. Cryptococcus
800 neoformans is a facultative intracellular pathogen in murine pulmonary infection.
801 *Infect Immun* **68**:4225–37. doi:10.1128/iai.68.7.4225-4237.200.
802 48. Esher SK, Ost KS, Kozubowski L, Yang DH, Kim MS, Bahn YS, Alspaugh JA,
803 Nichols CB. 2016. Relative contributions of prenylation and postprenylation
804 processing in *Cryptococcus neoformans* pathogenesis. *mSphere* **30**: e00084-15.
805 doi:10.1128/mSphere.00084-15.
806 49. Cox GM, Mukherjee J, Cole GT, Casadevall A, Perfect JR. 2000. Urease as a
807 virulence factor in experimental cryptococcosis. *Infect Immun* **68**:443–8.
808 doi:10.1128/iai.68.2.443-448.2000.
809 50. Nichols CB, Ferreyra J, Ballou ER, Alspaugh JA. 2009. Subcellular localization
810 directs signaling specificity of the Cryptococcus neoformans Ras1 protein.
811 *Eukaryot Cell* **8**:181–9. doi:10.1128/EC.00351-08.

812 51. Spiliotis ET, Kinoshita M, Nelson WJ. 2005. A mitotic septin scaffold required for
813 mammalian chromosome congression and segregation. *Science* **307**:1781–1785.
814 doi:10.1126/science.1106823.
815 52. Kinoshita M. 2006. Diversity of septin scaffolds. *Curr Opin Cell Biol* **18**:54–60.
816 doi:10.1016/j.ceb.2005.12.005.
817 53. Glomb O, Gronemeyer T. 2016. Septin organization and functions in budding
818 yeast. *Front Cell Dev Biol* **4**:123. doi:10.3389/fcell.2016.00123.
819 54. Finnigan GC, Duvalyan A, Liao EN, Sargsyan A, Thorner J. 2016. Detection of
820 protein-protein interactions at the septin collar in Saccharomyces cerevisiae using
821 a tripartite split-GFP system. *Mol Biol Cell* **27**:2708–25. doi:10.1091/mbc.E16-05-
822 0337.
823 55. Kelliher CM, Leman AR, Sierra CS, Haase SB. 2016. Investigating conservation
824 of the cell-cycle-regulated transcriptional program in the fungal pathogen,
825 Cryptococcus neoformans. *PLOS Genet* **12**:e1006453.
826 doi:10.1371/journal.pgen.1006453.
827 56. Qadota H, Python CP, Inoue SB, Arisawa M, Anraku Y, Zheng Y, Watanabe T,
828 Levin DE, Ohya Y. 1996. Identification of yeast Rho1p GTPase as a regulatory
829 subunit of 1,3-β-glucan synthase. *Science* **272**:279–281.
830 57. Cabib E, Roh DH, Schmidt M, Crotti LB, Varma A. 2001. The yeast cell wall and
831 septum as paradigms of cell growth and morphogenesis. *J Biol Chem* **276**:19679–
832 82. doi:10.1074/jbc.R000031200.
833 58. Chuang JS, Schekman RW. 1996. Differential trafficking and timed localization of
834 two chitin synthase proteins, Chs2p and Chs3p. *J Cell Biol* **135**:597-610.

doi:10.1083/jcb.135.3.597.

59. Banks IR, Specht CA, Donlin MJ, Gerik KJ, Levitz SM, Lodge JK. 2005. A chitin synthase and its regulator protein are critical for chitosan production and growth of the fungal pathogen Cryptococcus neoformans. *Eukaryot Cell* **4**:1902–12. doi:10.1128/EC.4.11.1902-1912.2005.

60. Reese AJ, Yoneda A, Breger JA, Beauvais A, Liu H, Griffith CL, Bose I, Kim MJ, Skau C, Yang S, Sefko JA, Osumi M, Latge JP, Mylonakis E, Doering TL. 2007. Loss of cell wall α(1-3) glucan affects Cryptococcus neoformans from ultrastructure to virulence. *Mol Microbiol* **63**:1385–98. doi:10.1111/j.1365-2958.2006.05551.

61. Carel C, Nukdee K, Cantaloube S, Bonne M, Diagne CT, Laval F, Daffé M, Zerbib D. 2014. Mycobacterium tuberculosis proteins involved in mycolic acid synthesis and transport localize dynamically to the old growing pole and septum. *PLoS One* **9**:e97148. doi:10.1371/journal.pone.0097148.

62. Mahmoud YA, Abu el Souod SM, Niehaus WG. 1996. Purification and characterization of fatty acid synthetase from Cryptococcus neoformans. *Mycopathologia* **136**:75–84.

63. Lynen F, Engeser H, Foerster EC, Fox JL, Hess S, Kresze GB, Schmitt T, Schreckenbach T, Siess E, Wieland F, Winnewisser W. 1980. On the Structure of Fatty Acid Synthetase of Yeast. *Eur J Biochem* **112**:431–442. doi:10.1111/j.1432-1033.1980.tb06105.

64. Schweizer E, Hofmann J. 2004. Microbial type I fatty acid synthases (FAS): Major players in a network of cellular FAS systems. *Microbiol Mol Biol Rev* **68**:501–17.

858 doi:10.1128/MMBR.68.3.501-517.2004.

859 65. Chayakulkeeree M, Rude TH, Toffaletti DL, Perfect JR. 2007. Fatty acid synthesis
860 is essential for survival of Cryptococcus neoformans and a potential fungicidal
861 target. *Antimicrob Agents Chemother* **51**:3537–45. doi:10.1128/AAC.00442-07.

862 66. Peng T, Golub TR, Sabatini DM. 2002. The immunosuppressant rapamycin
863 mimics a starvation-like signal distinct from amino acid and glucose deprivation.
864 *Mol Cell Biol* **22**:5575–84. doi:10.1128/mcb.22.15.5575-5584.2002.

865 67. Soliman GA. 2011. The integral role of mTOR in lipid metabolism. *Cell Cycle*
866 **10**:861–2. doi:10.4161/cc.10.6.14930.

867 68. Madeira JB, Masuda CA, Maya-Monteiro CM, Matos GS, Montero-Lomelí M,
868 Bozaquel-Morais BL. 2015. Torc1 inhibition induces lipid droplet replenishment in
869 yeast. *Mol Cell Biol* **35**:737–46. doi:10.1128/MCB.01314-14.

870 69. Davidson R, Laporte D, Wu JQ. 2015. Regulation of Rho-GEF Rgf3 by the
871 arrestin Art1 in fission yeast cytokinesis. *Mol Biol Cell* **26**:453–66.
872 doi:10.1091/mbc.E14-07-1252.

873 70. Saitoh S, Takahashi K, Nabeshima K, Yamashita Y, Nakaseko Y, Hirata A,
874 Yanagida M. 1996. Aberrant mitosis in fission yeast mutants defective in fatty acid
875 synthetase and acetyl CoA carboxylase. *J Cell Biol* **134**:949-61.
876 doi:10.1083/jcb.134.4.949.

877 71. Al-Feel W, DeMar JC, Wakil SJ. 2003. A Saccharomyces cerevisiae mutant strain
878 defective in acetyl-CoA carboxylase arrests at the G2/M phase of the cell cycle.
879 *Proc Natl Acad Sci U S A* **100**:3095–3100. doi:10.1073/pnas.0538069100.

880 72. Scaglia N, Tyekucheva S, Zadra G, Photopoulos C, Loda M. 2014. De novo fatty

881 acid synthesis at the mitotic exit is required to complete cellular division. *Cell*
882 *Cycle* **13**:859–68. doi:10.4161/cc.27767.
883 73. Callis J. 2014. The ubiquitination machinery of the ubiquitin system. *Arab B*
884 **12**:e0174. doi:10.1199/tab.0174.
885 74. Yu J, Deng R, Zhu HH, Zhang SS, Zhu C, Montminy M, Davis R, Feng GS. 2013.
886 Modulation of fatty acid synthase degradation by concerted action of p38 MAP
887 kinase, E3 ligase Cop1, and SH2-tyrosine phosphatase Shp2. *J Biol Chem*
888 **288**:3823–30. doi:10.1074/jbc.M112.397885.
889 75. Merlini L, Fraschini R, Boettcher B, Barral Y, Lucchini G, Piatti S. 2012. Budding
890 yeast Dma proteins control septin dynamics and the spindle position checkpoint
891 by promoting the recruitment of the Elm1 kinase to the bud neck. *PLoS Genet*
892 **8**:e1002670. doi:10.1371/journal.pgen.1002670.
893 76. Juanes MA, Piatti S. 2016. Control of formin distribution and actin cable assembly
894 by the E3 ubiquitin ligases Dma1 and Dma2. *Genetics* **204**:205–20.
895 doi:10.1534/genetics.116.189258.
896 77. Natter K, Leitner P, Faschinger A, Wolinski H, McCraith S, Fields S, Kohlwein SD.
897 2005. The spatial organization of lipid synthesis in the yeast Saccharomyces
898 cerevisiae derived from large scale green fluorescent protein tagging and high
899 resolution microscopy. *Mol Cell Proteomics* **4**:662–72. doi:10.1074/mcp.M400123-
900 MCP200.
901 78. Davis D, Edwards JE, Mitchell AP, Ibrahim AS. 2000. Candida albicans Rim101
902 pH response pathway is required for host-pathogen interactions. *Infect Immun*
903 **68**:5953–9. doi:10.1128/iai.68.10.5953-5959.2000.

79. Barlic J, Andrews JD, Kelvin AA, Bosinger SE, DeVries ME, Xu L, Dobransky T, Feldman RD, Ferguson SSG, Kelvin DJ. 2000. Regulation of tyrosine kinase activation and granule release through β-arrestin by Cxcr1. *Nat Immunol* 1:227–233. doi:10.1038/79767.

80. Gao H, Sun Y, Wu Y, Luan B, Wang Y, Qu B, Pei G. 2004. Identification of β-arrestin2 as a G protein-coupled receptor-stimulated regulator of NF-κB pathways. *Mol Cell* **14**:303–17.

81. Radin JN, Orihuela CJ, Murti G, Guglielmo C, Murray PJ, Tuomanen EI. 2005. β-Arrestin 1 participates in platelet-activating factor receptor-mediated endocytosis of Streptococcus pneumoniae. *Infect Immun* **73**:7827–35. doi:10.1128/IAI.73.12.7827-7835.2005.

82. Bhattacharyya S, Hope TJ, Young JA. 2011. Differential requirements for clathrin endocytic pathway components in cellular entry by Ebola and Marburg glycoprotein pseudovirions. *Virology* **419**:1–9. doi:10.1016/j.virol.2011.07.018.

83. Vines CM, Revankar CM, Maestas DC, LaRusch LL, Cimino DF, Kohout TA, Lefkowitz RJ, Prossnitz ER. 2003. N-formyl peptide receptors internalize but do not recycle in the absence of arrestins. *J Biol Chem* **278**:41581–4. doi:10.1074/jbc.C300291200.

84. Ost KS, Esher SK, Leopold Wager CM, Walker L, Wagener J, Munro C, Wormley FL, Alspaugh JA. 2017. Rim pathway-mediated alterations in the fungal cell wall influence immune recognition and inflammation. *MBio* **8**:e02290-16. doi:10.1128/mBio.02290-16.

85. Toffaletti DL, Rude TH, Johnston SA, Durack DT, Perfect JR. 1993. Gene transfer

in *Cryptococcus neoformans* by use of biolistic delivery of DNA. *J Bacteriol* **175**:1405–11. doi:10.1128/jb.175.5.1405-1411.1993.

86. Kim MS, Kim SY, Jung KW, Bahn YS. 2012. Targeted gene disruption in Cryptococcus neoformans using double-joint PCR with split dominant selectable markers. *Methods Mol Biol* **845**:67-84. doi:10.1007/978-1-61779-539-8_5.

87. Chun CD, Madhani HD. 2010. Applying genetics and molecular biology to the study of the human pathogen *Cryptococcus neoformans*. *Methods Enzymol* **470**:797-831. doi:10.1016/S0076-6879(10)70033-1.

88. Murashige T, Skoog F. 1962. A revised medium for rapid growth and bio assays with tobacco tissue cultures. *Physiol Plant* **15**:473–497. doi:10.1111/j.1399-3054.1962.tb08052.

89. Schneider CA, Rasband WS, Eliceiri KW. 2012. NIH image to ImageJ: 25 years of image analysis. *Nat Methods* **9**:671–675. doi:10.1038/nmeth.2089.

90. Abràmoff MD, Magalhães PJ, Ram SJ. 2004. Image processing with ImageJ. *Biophotonics Int* **11**:36-42.

91. Pfaller MA, Rinaldi MG, Galgiani JN, Bartlett MS, Body BA, Espinel-Ingroff A, Fromtling RA, Hall GS, Hughes CE, Odds FC. 1990. Collaborative investigation of variables in susceptibility testing of yeasts. *Antimicrob Agents Chemother* **34**:1648–54. doi:10.1128/aac.34.9.1648.

92. Clinical and Laboratory Standards Institute (CLSI). 2008. Reference method for broth dilution antifungal susceptibility testing of yeasts; Approved Standard-Third Edition. Clinical and Laboratory Standards Institute, Wayne, PA.

93. Perfect JR, Lang SD, Durack DT. 1980. Chronic cryptococcal meningitis: A new

950 experimental model in rabbits. *Am J Pathol* **101**:177–94.

951 94. Nielsen K, Cox GM, Wang P, Toffaletti DL, Perfect JR, Heitman J. 2003. Sexual

952 cycle of Cryptococcus neoformans var. grubii and virulence of congenic a and α

953 isolates. *Infect Immun* **71**:4831–41. doi:10.1128/iai.71.9.4831-4841.2003.

954 95. Fraser JA, Subaran RL, Nichols CB, Heitman J. 2003. Recapitulation of the

955 sexual cycle of the primary fungal pathogen Cryptococcus neoformans var. gattii:

956 Implications for an outbreak on Vancouver Island, Canada. *Eukaryot Cell* **2**:1036–

957 45. doi:10.1128/ec.2.5.1036-1045.2003.

958 96. McDade HC, Cox GM. 2001. A new dominant selectable marker for use in

959 Cryptococcus neoformans. *Med Mycol* **39**:151-4. doi:10.1080/mmy.39.1.151.154.

960 97. Price MS, Nichols CB, Alspaugh JA. 2008. The Cryptococcus neoformans Rho-

961 GDP dissociation inhibitor mediates intracellular survival and virulence. *Infect*

962 *Immun* **76**:5729–37. doi:10.1128/IAI.00896-08.

963 **TABLE 1**. The most abundant 30 proteins identified as potential Ali1-GFP interactors in

964 YPD medium[a]

Gene ID	Gene Name	Gene Product	Average Peptide Count (APC)	Percent of APC identified in WT
CNAG_02099	*FAS1*	Fatty acid synthase, beta subunit	9.0	0.0
CNAG_02100	*FAS2*	Fatty acid synthase, alpha subunit	8.7	11.5
CNAG_02748		UTP-glucose-1-phosphate uridylyltransferase	8.7	11.5
CNAG_07373		Carbamoyl-phosphate synthase, large subunit	8.0	0.0
CNAG_03944		Chaperone regulator	6.7	15.0
CNAG_03358		Phosphoglycerate kinase	6.0	0.0
CNAG_04441		Polyadenylate-binding protein, cytoplasmic and nuclear	6.0	16.7
CNAG_01464	*FHB1*	Flavohemoglobin	5.7	17.6
CNAG_00418		S-adenosylmethionine synthase	5.3	18.8
CNAG_01586		F-type H-transporting ATPase, B subunit	5.0	0.0
CNAG_02545		Inorganic pyrophosphatase	5.0	0.0
CNAG_04659		Pyruvate decarboxylase	4.7	0.0
CNAG_02928		Large subunit ribosomal protein L5e	4.3	0.0
CNAG_05759		Acetyl-CoA carboxylase/biotin carboxylase	4.0	0.0
CNAG_07363		Isocitrate dehydrogenase, NAD-dependent	4.0	0.0
CNAG_02673		NAD dependent epimerase/dehydratase	3.7	0.0
CNAG_02811		Small subunit ribosomal protein S29	3.7	0.0
CNAG_07745	*MPD1*	Alcohol dehydrogenase, propanol-preferring	3.3	0.0
CNAG_00176		Glutamate carboxypeptidase	3.3	0.0
CNAG_01404		Hsp71-like protein	3.3	0.0
CNAG_02500		Calnexin	3.0	0.0
CNAG_02991		Cofilin	3.0	0.0
CNAG_02943		Cytoplasmic protein	3.0	0.0
CNAG_03588	*LYS2*	L-aminoadipate-semialdehyde dehydrogenase	3.0	0.0
CNAG_02736		T-complex protein 1, theta subunit	3.0	0.0
CNAG_03765	*TPS2*	Trehalose-phosphatase	3.0	0.0
CNAG_00136		Ubiquitin-activating enzyme E1	3.0	0.0
CNAG_07558		Uncharacterized protein	3.0	0.0
CNAG_06112		Carbamoyl-phosphate synthase arginine-specific, large chain	2.7	0.0
CNAG_00879		Glutamate dehydrogenase	2.7	0.0

965 [a] The average peptide count (APC) was calculated by averaging the exclusive unique

966 peptide counts for each potential interactor across three biological replicates. The

967 percent of APC identified in the WT immunoprecipitation was calculated by dividing the

APC of each potential interactor by the exclusive unique peptide count found in the WT immunoprecipitation. All potential protein interactors with an APC of 2 or more, as well as less than 20% of the APC identified in the WT immunoprecipitation, were considered to be unique interactors with Ali1-GFP. These potential protein interactors are prioritized by APC (most to least) and percentage of APC identified in the WT control (lowest to highest).

974 **TABLE 2**. The most abundant 30 proteins identified as potential Ali1-GFP interactors in

975 TC medium[a]

Gene ID	Gene Name	Gene Product	Average Peptide Count (APC)	Percent of APC identified in WT
CNAG_02099	*FAS1*	Fatty acid synthase, beta subunit	19.3	0.0
CNAG_02100	*FAS2*	Fatty acid synthase, alpha subunit	16.7	6.0
CNAG_04327		Uncharacterized protein	10.3	9.7
CNAG_05355	*RSP5*	E3 ubiquitin-protein ligase	6.0	0.0
CNAG_05978		Glutamate-tRNA ligase	6.0	16.7
CNAG_03588	*LYS2*	L-aminoadipate-semialdehyde dehydrogenase	6.0	16.7
CNAG_03701		3-phosphoshikimate 1-carboxyvinyltransferase	5.7	17.6
CNAG_00743		Imidazoleglycerol phosphate synthase, cyclase subunit	5.3	0.0
CNAG_07561		6-phosphogluconate dehydrogenase, decarboxylating I	5.3	18.8
CNAG_06175		26S proteasome, regulatory subunit N2	4.7	0.0
CNAG_01216		6-phosphogluconolactonase	4.0	0.0
CNAG_00602		Eukaryotic translation initiation factor 3, subunit I	4.0	0.0
CNAG_00136		Ubiquitin-activating enzyme E1	4.0	0.0
CNAG_06666		Alpha-1,4 glucan phosphorylase	3.7	0.0
CNAG_02565		Homoaconitase, mitochondrial	3.7	0.0
CNAG_02035		Triosephosphate isomerase	3.7	0.0
CNAG_05650	*UBP5*	Ubiquitin carboxyl-terminal hydrolase 7	3.7	0.0
CNAG_00708		Pre-mRNA-splicing factor Slt11	3.3	0.0
CNAG_01981		Sulfide:quinone oxidoreductase	3.3	0.0
CNAG_03249		THO complex, subunit 4	3.3	0.0
CNAG_00649		Tryptophan synthase, beta subunit	3.3	0.0
CNAG_02858	*ADE12*	Adenylosuccinate synthetase	3.0	0.0
CNAG_01189		DNA-directed RNA polymerase I, subunit RPA1	3.0	0.0
CNAG_02545		Inorganic pyrophosphatase	3.0	0.0
CNAG_04976		Zuotin	3.0	0.0
CNAG_04951		3-deoxy-7-phosphoheptulonate synthase	2.7	0.0
CNAG_02500		Calnexin	2.7	0.0
CNAG_06730	*GSK3*	CMGC/GSK protein kinase	2.7	0.0
CNAG_00700		Phosphoribosylaminoimidazolecarboxamide formyltransferase/IMP cyclohydrolase	2.7	0.0
CNAG_02315		Ubiquinol-cytochrome c reductase, iron-sulfur subunit	2.7	0.0

976 [a] The average peptide count (APC) was calculated by averaging the exclusive unique

977 peptide counts for each potential interactor across three biological replicates. The

978 percent of APC identified in the WT immunoprecipitation was calculated by dividing the

APC of each potential interactor by the exclusive unique peptide count found in the WT immunoprecipitation. All potential protein interactors with an APC of 2 or more, as well as less than 20% of the APC identified in the WT immunoprecipitation, were considered to be unique interactors with Ali1-GFP. These potential protein interactors are prioritized by APC (most to least) and percentage of APC identified in the WT control (lowest to highest).

985 **TABLE 3.** Strains used in this study

Strain	Genotype	Source
H99	*MAT*α	(93)
KN99a	*MAT*a	(94)
KS120	*MAT*α *ali1*Δ::*NEO*	(25)
CLT6	*MAT*α *ali1*Δ::*NEO* + *ALI1-NAT*	This study
CLT7	*MAT*α *ali1*Δ::*NEO* + *H-ALI1-GFP-NAT*	This study
CBN327	*MAT*a *GAL7-mCherry-RAS1-NEO*	This study
CBN486	*MAT*α *ali1*Δ::*NEO* + *H-ALI1-GFP-NAT* + *GAL7-mCherry-RAS1-NEO*	This study
LK001	*MAT*α *CDC10-mCherry-NEO*	(34)
CLT42	*MAT*α *ali1*Δ::*NAT* + *CDC10-mCherry-NEO*	This study
KS96-2	*MAT*α *ali2*Δ::*NAT*	(25)
CLT67	*MAT*α *ali2*Δ::*NAT* + *ALI2-GFP-NEO*	This study
CLT8	*MAT*α *ali3*Δ::*NAT*	Madhani, 2015
CLT32	*MAT*a *ali3*Δ::*NAT*	This study
CLT62	*MAT*α *ali3*Δ::*NAT* + *ALI3-NEO*	This study
CLT9	*MAT*α *ali4*Δ::*NAT*	Madhani, 2015
CLT63	*MAT*α *ali4*Δ::*NAT* + *ALI4-NEO*	This study
KS97-2	*MAT*α *ali1*Δ::*NEO* + *ali2*Δ::*NAT*	(25)
CLT35	*MAT*a *ali3*Δ::*NAT* + *ali4*Δ::*NAT*	This study
CLT56	*MAT*a *ali1*Δ::*NEO* + *ali2*Δ::*NAT* + *ali3*Δ::*NAT* + *ali4*Δ::*NAT* #1	This study
CLT57	*MAT*a *ali1*Δ::*NEO* + *ali2*Δ::*NAT* + *ali3*Δ::*NAT* + *ali4*Δ::*NAT* #2	This study
CLT58	*MAT*a *ali1*Δ::*NEO* + *ali2*Δ::*NAT* + *ali3*Δ::*NAT* + *ali4*Δ::*NAT* #3	This study

986

987 **TABLE 4**. Plasmids used in this study

Plasmid	ORF	Backbone	Source
pJAF	Neomycin resistance cassette (*NEO*)		(95)
pCH233	Nourseothricin resistance cassette (*NAT*)		(96)
pCT1	*ALI1* (including promoter and terminator); *NAT*	pCH233	This study
pCN20	Histone *H3* promoter; *NAT*	pCH233	(97)
pKS85	Histone *H3* promoter; *RRA1*; *GFP*; *RRA1* (terminator only); *NAT*	pCH233	(26)
pCT3	Histone *H3* promoter; *ALI1*; *GFP*; *RRA1* (terminator only); *NAT*	pUC19	This study
pCT11	*ALI2* (including promoter); *GFP*; *FKS1* (terminator only)*; NEO*	pUC19	This study
pCT8	*ALI3* (including promoter and terminator); *NEO*	pJAF	This study
pCT10	*ALI4* (including promoter and terminator); *NEO*	pJAF	This study

988

989 **TABLE 5**. Primers used in this study

Primer name	Primer sequence (5'-3')	Purpose
Deletion constructs		
AA3254	GAGGACTACTTGGGCGTCAA	*ali1*Δ primer 1
AA3255	GTCATAGCTGTTTCCTGCTGTCGGACCGTGTTTATCG	*ali1*Δ primer 2
AA3256	CGATAAACACGGTCCGACAGCAGGAAACAGCTATGAC	*ali1*Δ primer 3
AA3257	ATATTATAAGTTAGAGGTTAGGTTTTCCCAGTCACGAC	*ali1*Δ primer 4
AA3258	GTCGTGACTGGGAAAACCTAACCTCTAACTTATAATAT	*ali1*Δ primer 5
AA3259	GGACGGGAGTGTAATGAGGA	*ali1*Δ primer 6
AA3505	CTGAGCGGTGTCCTTTTCTC	*ali2*Δ primer 1
AA3506	GTCATAGCTGTTTCCTGGGTGTGGGTGTGGTTGTCGTGGT	*ali2*Δ primer 2
AA3507	ACCACGACAACCACACCCACACCCAGGAAACAGCTATGAC	*ali2*Δ primer 3
AA3508	GTATATCTAGATTGAACAACTAAGTTTTCCCAGTCACGAC	*ali2*Δ primer 4
AA3509	GTCGTGACTGGGAAAACTTAGTTGTTCAATCTAGATATAC	*ali2*Δ primer 5
AA3510	TTTCAGTTCCGAGGTGCTCT	*ali2*Δ primer 6
AA4096	AAGGTGTTCCCCGACGACGAATCG	*NAT* split marker F
AA4097	AACTCCGTCGCGAGCCCCATCAAC	*NAT* split marker R
AA3934	TCGATGCGATGTTTCGCT	*NEO* split marker F
AA3935	CCTGAATGAACTGCAGGA	*NEO* split marker R
Cloning		
AA5124	TACCGAGCTCGGATCCGTGTCGTTAGCGGACTCGGTATCT	*ALI1* fragment F
AA5125	CGTTACTAGTGGATCCTCCGCTACATAACCACCATCCCTG	*ALI1* fragment R
AA5192	GAGCTCGGTACCCGGGGATCGGCAGATACGATATGTTGGCGC	*ALI1-GFP* fragment 1 F
AA5185	GAGAGGGCATGGTGATAGATGTGTTGTGGTGTTG	*ALI1-GFP* fragment 1 R
AA5186	ATCTATCACCATGCCCTCTCGTTGGATCCCAAGC	*ALI1-GFP* fragment 2 F
AA5187	TGCTCACCATTGCTCCTGTCGGCGCCCC	*ALI1-GFP* fragment 2 R
AA5188	GACAGGAGCAATGGTGAGCAAGGGCGAGG	*ALI1-GFP* fragment 3 F
AA5204	CAGGTCGACTCTAGAGGATCCTGCGAGGATGTGAGCTGG	*ALI1-GFP* fragment 3 R
AA5518	AATTCGAGCTCGGTACCCGGGGATCGACCATCAACGCCAGCGTATTAAC	*ALI2-GFP* fragment 1 F
AA5519	CTTGCTCACCATATCTCTGAGCCTGTTGCGG	*ALI2-GFP* fragment 1 R
AA5520	CAGGCTCAGAGATATGGTGAGCAAGGGCGAG	*ALI2-GFP* fragment 2 F
AA5521	GCCTGCAGGTCGACTCTAGAGGATCCTGCGAGGATGTGAGCTG	*ALI2-GFP* fragment 2 R
AA4424	GATCCTCTAGAGTCGACCTG	pUC19 F
AA4425	GATCCCCGGGTACCGAGCTC	pUC19 R
AA5415	CGTCGCACTAGTATTGTGTAGCGGCGCTATAGTG	*ALI3* fragment F
AA5416	CGTCGCACTAGTCAAGAATGGTGACACTGCCAAC	*ALI3* fragment R
AA5417	CGTCGCACTAGTTTCTCCTTGCGGAGGCTTATTAG	*ALI4* fragment F
AA5418	CGTCGCACTAGTACAACTACAGCTCTGGCATCTAG	*ALI4* fragment R

990

991 **FIGURE 1**. The *C. neoformans* arrestin proteins. The arrestin proteins within the *C.*
992 *neoformans* proteome – Ali1, Ali2, Ali3, and Ali4 – were identified by the presence of the
993 conserved β-sheet-rich arrestin domains. If present, the N-terminal arrestin domain
994 (yellow), the C-terminal arrestin domain (blue), and any potential ubiquitin ligase binding
995 sequences, or PxY sequences (black), are indicated for each arrestin protein. Protein
996 and domain sizes are depicted to scale (aa = amino acids).

FIGURE 2. Ali1 subcellular localization patterns. A. The WT and Ali1-GFP strains were incubated in YPD medium at 30°C (above) or TC medium at 37°C, and Ali1-GFP was localized by epifluorescence microscopy (Zeiss Axio Imager A1). Ali1-GFP localization to the septum (arrowheads) and poles (arrows) of budding yeasts is depicted. B. To determine the relative enrichment of Ali1-GFP in different cellular fractions, WT and Ali1-GFP total cell lysates (T) were subjected to ultracentrifugation (30,000 $\times$ g) to isolate the soluble (S) and insoluble (I) cellular fractions. Samples were analyzed by western blotting using an anti-GFP antibody. The estimated size of Ali1-GFP is approximately 122 kDa. C. The dependence of Ali1-GFP localization on the Ras1 signaling pathway was determined using galactose-inducible expression of the *RAS1* transcript. Cells were incubated in YPGal (WT) or YPD (*ras1*Δ) media. Ali1-GFP localization to the septum (arrowheads) and poles (arrows) of budding yeasts was observed using epifluorescence microscopy (Zeiss Axio Imager A1). D. The frequency of Ali1-GFP localization to the septum and poles was quantified in the presence and absence of Ras1. The percentage of actively budding cells that displayed Ali1-GFP localization to the septum and/or poles was calculated in both YPGal (WT) and YPD (*ras1*Δ) conditions. A minimum of 600 cells were analyzed in both YPGal (WT) and YPD (*ras1*Δ) conditions across three biological replicates (n = 3). Error bars represent the standard error of the mean (SEM). Log transformation was used to normally distribute the data for statistical analysis (*Student's *t*-test $p < 0.05$).

FIGURE 3. Cellular morphology of the *ali1*Δ mutant. A. The WT, *ali1*Δ mutant, and *ali1*Δ + *ALI1* strains were incubated in YPD medium at either 30°C or 39°C and subsequently imaged by DIC microscopy (Zeiss Axio Imager A1). The *ali1*Δ mutant cells displaying morphological defects, such as elongated cells (asterisk), wide bud necks (arrowhead), and cytokinesis failure (arrow), are indicated. B. The percentage of total cells displaying morphological defects at 39°C was quantified for each strain. A minimum of 600 cells were analyzed across three biological replicates (n = 3). Error bars represent the SEM. Log transformation was used to normally distribute the data for statistical analysis (**One-way ANOVA $p < 0.01$; ns = not significant). C. The septin protein, Cdc10, was localized by visualization of the Cdc10-mCherry fusion protein in both the WT and the *ali1*Δ mutant backgrounds after incubation in YPD medium at 30°C (above) or 37°C. The Cdc10-mCherry fusion protein was localized using epifluorescence microscopy (Zeiss Axio Imager A1).

1030 **FIGURE 4**. The effects of lipid supplementation on the *ali1*Δ mutant. Serial dilutions of
1031 the WT, *ali1*Δ mutant, and *ali1*Δ + *ALI1* strains were incubated on YPD medium; YPD
1032 with caffeine (1 mg/mL); YPD with caffeine, ox bile (10 mg/mL), and Tween 60 (1%);
1033 and YPD with caffeine and glycerol (0.4%). These strains were incubated at 30°C (A)
1034 and 37°C (B) and monitored visually for growth.

FIGURE 5. Virulence contributions of the *C. neoformans* arrestin family. A. The WT, *ali1*Δ mutant, and *ali1*Δ + *ALI1* strains were co-incubated with J774A.1 murine macrophages at a multiplicity of infection (MOI) = 1 for 24 hours. Survival of the strains was assessed by quantitative culture, and the percentage of recovered colony-forming units (CFU) was normalized to the WT strain. This experiment was performed with six biological replicates (n = 6). Error bars represent the SEM. Log transformation was used to normally distribute the data for statistical analysis (One-way ANOVA; ns = not significant). B. Female C57BL/6 mice (n = 10) were intranasally inoculated with 10^4 CFU of the WT, *ali1*Δ mutant, or *ali1*Δ + *ALI1* strains. Mouse survival was tracked for 50 days post-infection (Log-rank test; ns = not significant). C. The WT strain, the *MAT*a KN99 strain, and three isogenic but independent arrestin null mutants (all also *MAT*a) were co-incubated with J774A.1 murine macrophages at a MOI = 1 for 24 hours. Survival of the strains was assessed by quantitative culture, and the percentage of recovered CFU was normalized to the WT strain. This experiment was performed with four biological replicates (n = 4). Error bars represent the SEM. Log transformation was used to normally distribute the data for statistical analysis (*One-way ANOVA $p < 0.05$; **One-way ANOVA $p < 0.01$). D. Female C57BL/6 mice (n = 10) were intranasally inoculated with 10^4 CFU of the WT strain and a representative arrestin null mutant, *ali1*Δ*ali2*Δ*ali3*Δ*ali4*Δ - #2 (CLT57). Mouse survival was tracked for 50 days post-infection (****Log-rank test $p < 0.0001$).

FIGURE 6. The *C. neoformans* arrestin mutant phenotypes. Serial dilutions of the WT strain, each individual arrestin mutant, and three independent arrestin null mutants were incubated on YPD medium with the following growth conditions/additives: 30°C, 39°C, caffeine (1 mg/mL), SDS (0.03%), high salt (1.5 M NaCl), and alkaline pH (pH 8). Cells were monitored visually for growth. The *ali1*Δ mutant exhibits modest susceptibility to caffeine. This phenotype is shared by, but markedly enhanced in, the *ali2*Δ mutant. The *ali2*Δ mutant also displays sensitivity to high salt. The *ali3*Δ mutant has modest growth defects at 39°C, as well as resistance to SDS. The *ali4*Δ mutant shares this SDS resistance phenotype, although it is enhanced compared to the *ali3*Δ mutant. The arrestin null mutants display reduced growth in the presence of 39°C, caffeine, and salt, but enhanced growth in the presence of SDS and alkaline pH.

FIGURE 7. Working model of Ali1 adaptor function. We propose that Ali1 (yellow/blue) acts as an adaptor protein to aid in the localization of the Fas1 and Fas2 fatty acid synthase complex (red) to the septum and poles of actively dividing cells, possibly in a ubiquitin-mediated manner through interactions with the E3 ubiquitin ligase Rsp5 (green). This process occurs to help meet the increased, stress-induced need for lipid synthesis and deposition at these sites. In the *ali1*Δ mutant strain, Fas1 and Fas2 are unable to localize, or are delayed in their localization, to the septum and poles during cell division. As a result, lipid synthesis and deposition at these sites is impaired. This causes localized cell surface defects at the poles in the resulting cells, likely explaining the cytokinesis defects and caffeine sensitivity phenotypes of the *ali1*Δ mutant.

1076 **TABLE S1**. Primary amino acid sequence homology between the *C. neoformans*

1077 arrestins and *S. cerevisiae* arrestins[a]

1078

1079 [a] The blastp and PSI-BLAST programs were used to identify amino acid sequence

1080 conservation. Alignments with an E value less than 1 were determined to be significant

1081 (N/A = not applicable).

1082 **TABLE S2**. Primary amino acid sequence homology between the *C. neoformans*

1083 arrestins and human arrestins[a]

1084

1085 [a] The blastp and PSI-BLAST programs were used to identify amino acid sequence

1086 conservation. Alignments with an E value less than 1 were determined to be significant

1087 (N/A = not applicable).

1088 **TABLE S3**. A total of 1,122 proteins were identified as potential interactors of Ali1-GFP[a]

1089

1090 [a] All identified *C. neoformans* proteins are included, along with the exclusive unique

1091 peptide count for each protein in each replicate.

TABLE S4. The 59 biologically-relevant proteins identified as potential interactors of Ali1-GFP in YPD medium[a]

[a] The average peptide count (APC) was calculated by averaging the exclusive unique peptide counts for each potential interactor across three biological replicates. The percent of APC identified in the WT immunoprecipitation was calculated by dividing the APC of each potential interactor by the exclusive unique peptide count found in the WT immunoprecipitation. All potential protein interactors with an APC of 2 or more, as well as less than 20% of the APC identified in the WT immunoprecipitation, were considered to be unique interactors with Ali1-GFP. These potential protein interactors are prioritized by APC (most to least) and percentage of APC identified in the WT control (lowest to highest).

TABLE S5. The 62 biologically-relevant proteins identified as potential interactors of Ali1-GFP in TC medium[a]

[a] The average peptide count (APC) was calculated by averaging the exclusive unique peptide counts for each potential interactor across three biological replicates. The percent of APC identified in the WT immunoprecipitation was calculated by dividing the APC of each potential interactor by the exclusive unique peptide count found in the WT immunoprecipitation. All potential protein interactors with an APC of 2 or more, as well as less than 20% of the APC identified in the WT immunoprecipitation, were considered to be unique interactors with Ali1-GFP. These potential protein interactors are prioritized by APC (most to least) and percentage of APC identified in the WT control (lowest to highest).

FIGURE S1. Cellular morphology of the *ali1*Δ mutant at 30°C. The WT, *ali1*Δ mutant, and *ali1*Δ + *ALI1* strains were incubated in YPD medium at 30°C, imaged by DIC microscopy (Zeiss Axio Imager A1), and quantified for the frequency of cytokinesis defects. The percentage of total cells displaying morphological defects at 30°C was quantified for each strain. A minimum of 600 cells were analyzed across three biological replicates (n = 3). Error bars represent the SEM. Log transformation was used to normally distribute the data for statistical analysis (One-way ANOVA; ns = not significant).

FIGURE S2. Complementation phenotypes of the individual arrestin mutants. A. Serial dilutions of the WT, *ali2*Δ mutant, and the *ali2*Δ + *ALI2-GFP* strains were incubated on YPD medium, YPD with caffeine (1 mg/mL), and YPD with high salt (1.5 M NaCl). These strains were incubated at 30°C and monitored visually for growth. B. Serial dilutions of the WT, *ali3*Δ mutant, and the *ali3*Δ + *ALI3* strains were incubated on YPD medium incubated at 30°C, YPD medium incubated at 39°C, and YPD with SDS (0.03%) incubated at 30°C. These strains were monitored visually for growth. C. Serial dilutions of the WT, *ali4*Δ mutant, and the *ali4*Δ + *ALI4* strains were incubated on YPD medium and YPD with SDS (0.03%). These strains were incubated at 30°C and monitored visually for growth.

FIGURE S3. Virulence contributions of Ali2. The WT, *ali2*Δ mutant, *ali2*Δ + *ALI2-GFP*, and *ali1*Δ*ali2*Δ mutant strains were co-incubated with J774A.1 murine macrophages at a MOI = 1 for 24 hours. Survival of the strains was assessed by quantitative culture, and the percentage of recovered CFU was normalized to the WT strain. This experiment was performed with five biological replicates (n = 5). Error bars represent the SEM. Log transformation was used to normally distribute the data for statistical analysis (*One-way ANOVA $p < 0.05$; ****One-way ANOVA $p < 0.0001$; ns = not significant).

FIGURE S4. The effects of lipid supplementation on the arrestin null mutants. A. Serial dilutions of the WT and arrestin null mutant strains were incubated on YPD medium at 30°C; YPD at 39°C; YPD with glycerol (0.4%) at 39°C; and YPD with sorbitol (1M) at 39°C. These strains were monitored visually for growth. B. Serial dilutions of the WT and arrestin null mutant strains were incubated on YPD medium; YPD with caffeine (1 mg/mL); YPD with caffeine and glycerol (0.4%); and YPD with caffeine and sorbitol (1M). These strains were incubated at 30°C and monitored visually for growth.

1148 **FILE S1**. Supplementary materials and methods

Figure 1

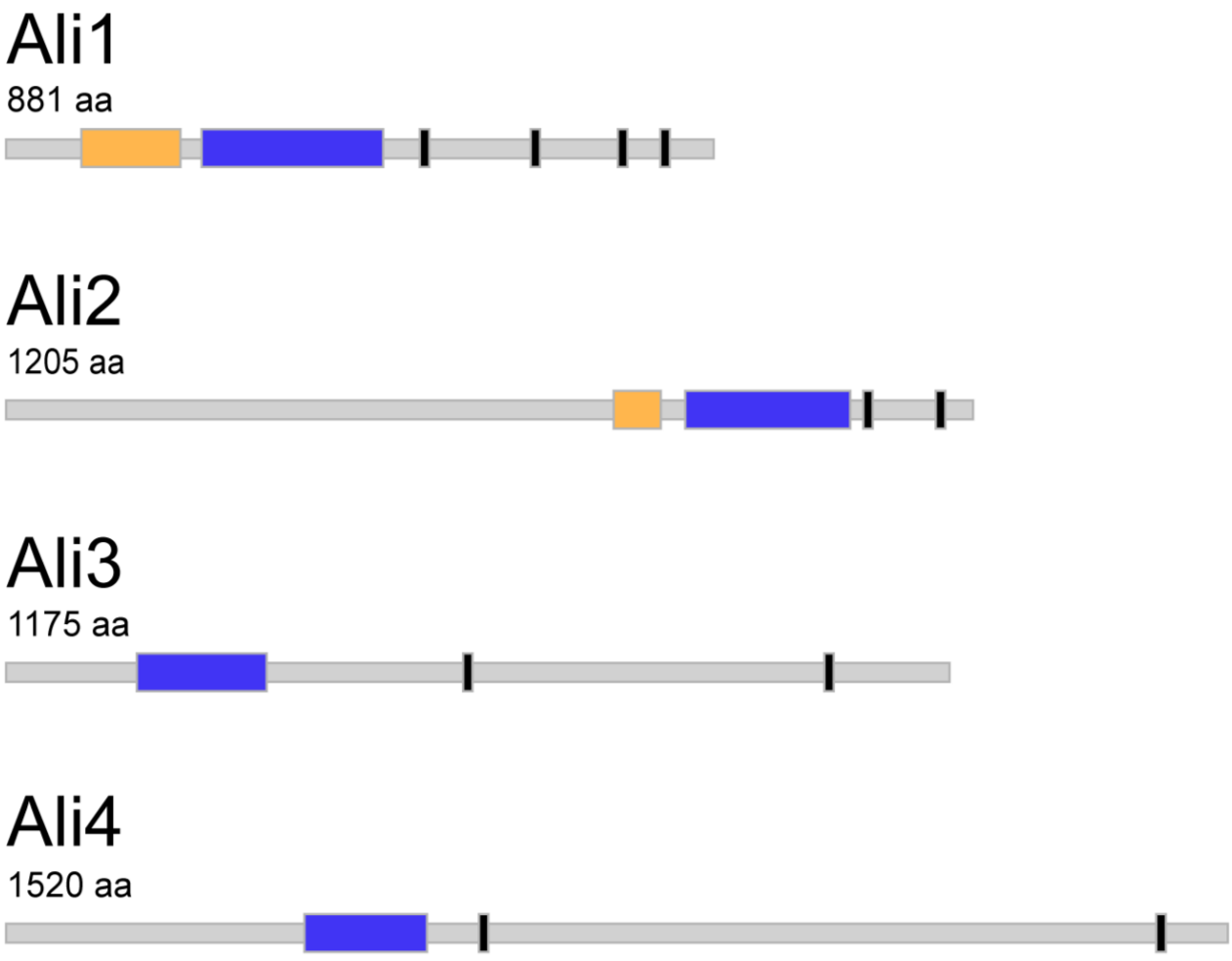

Figure 2

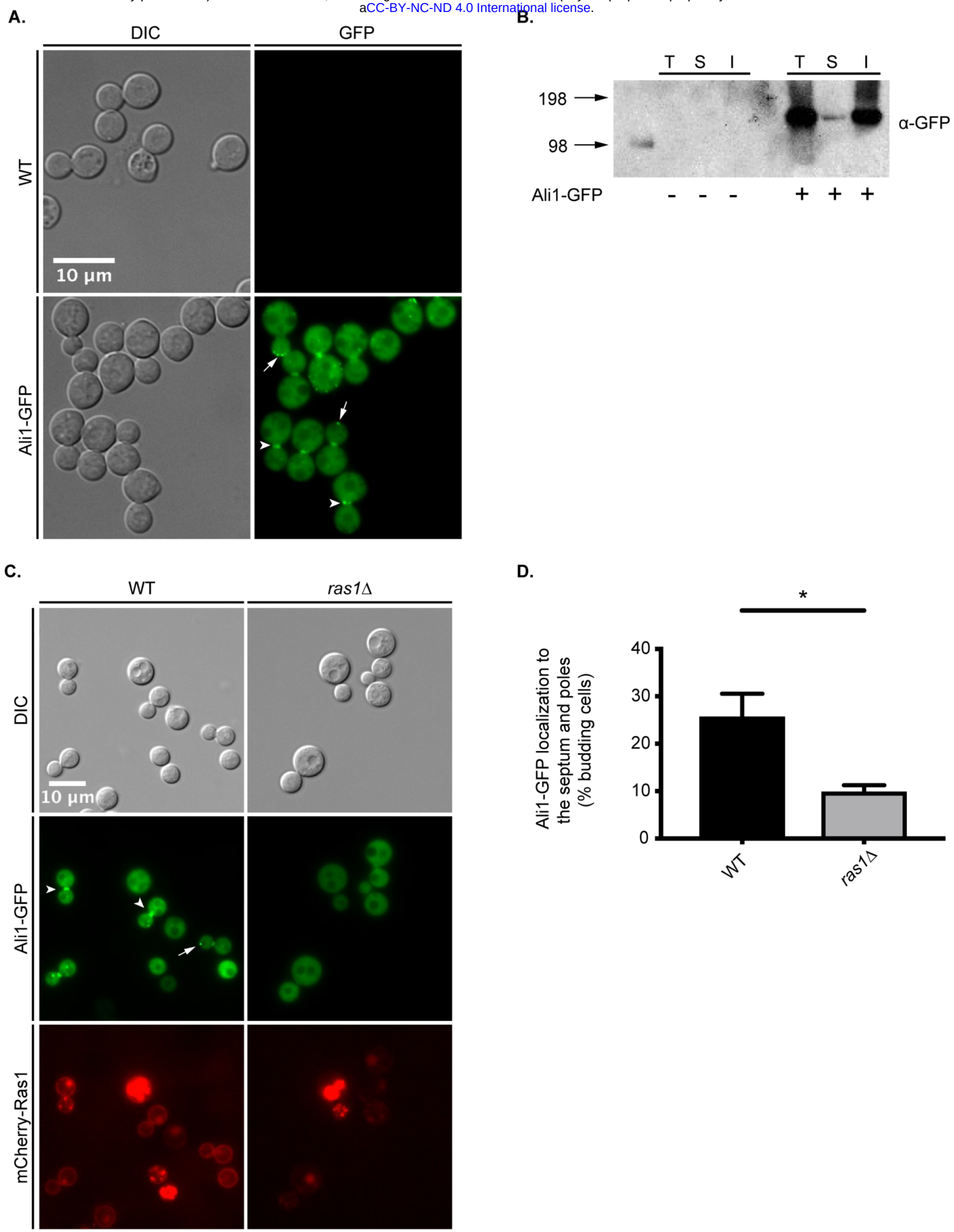

Figure 3

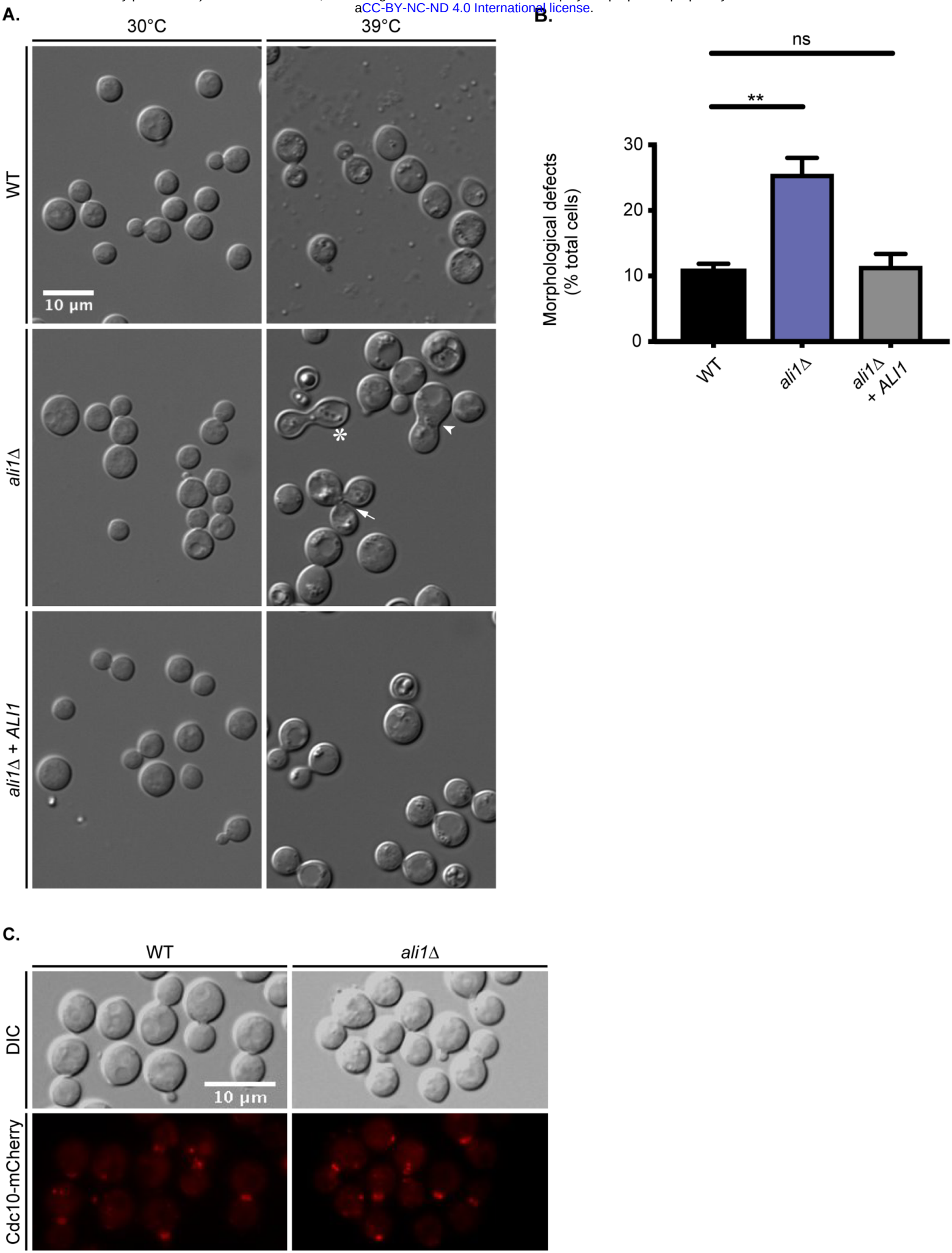

Figure 4

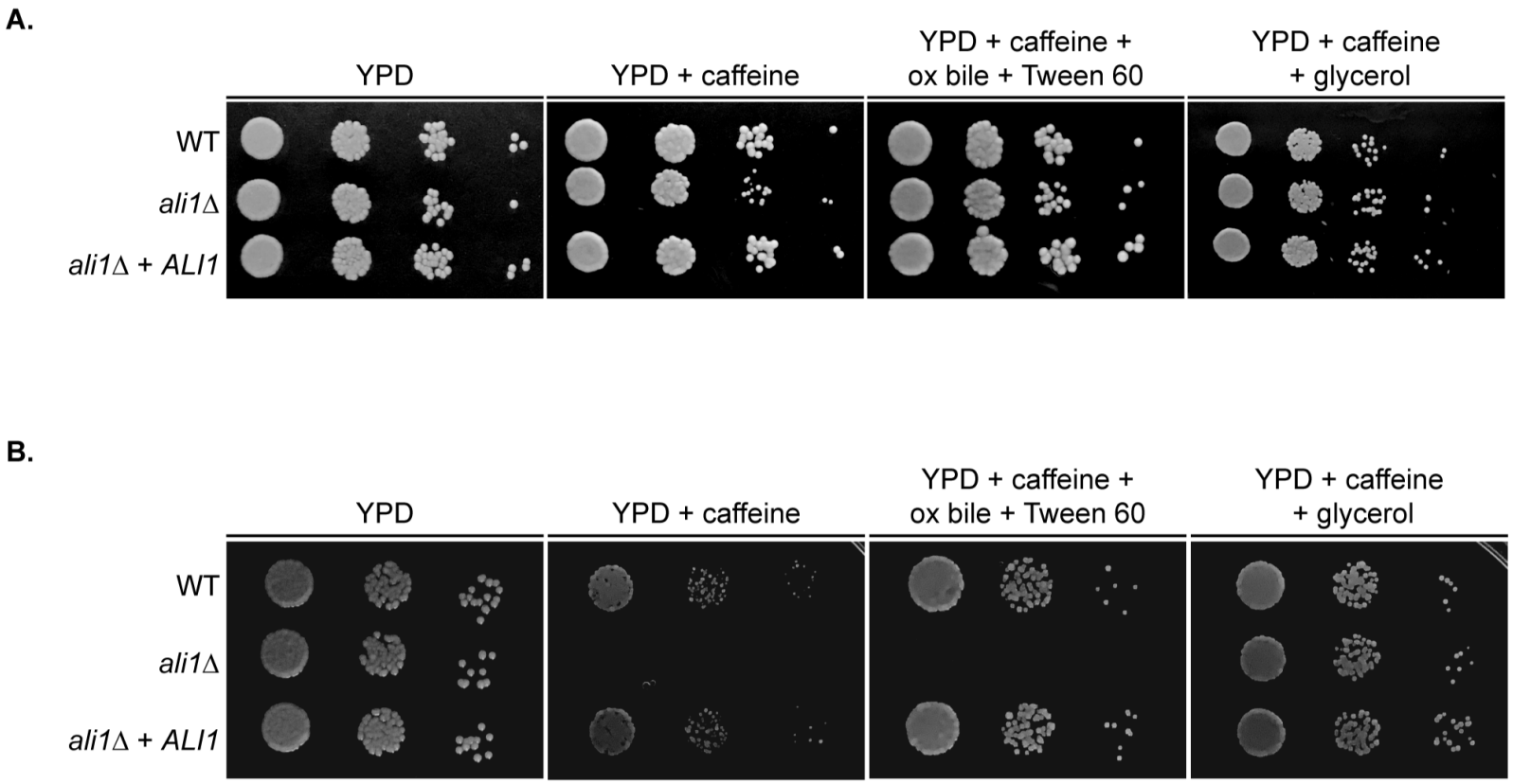

Figure 5

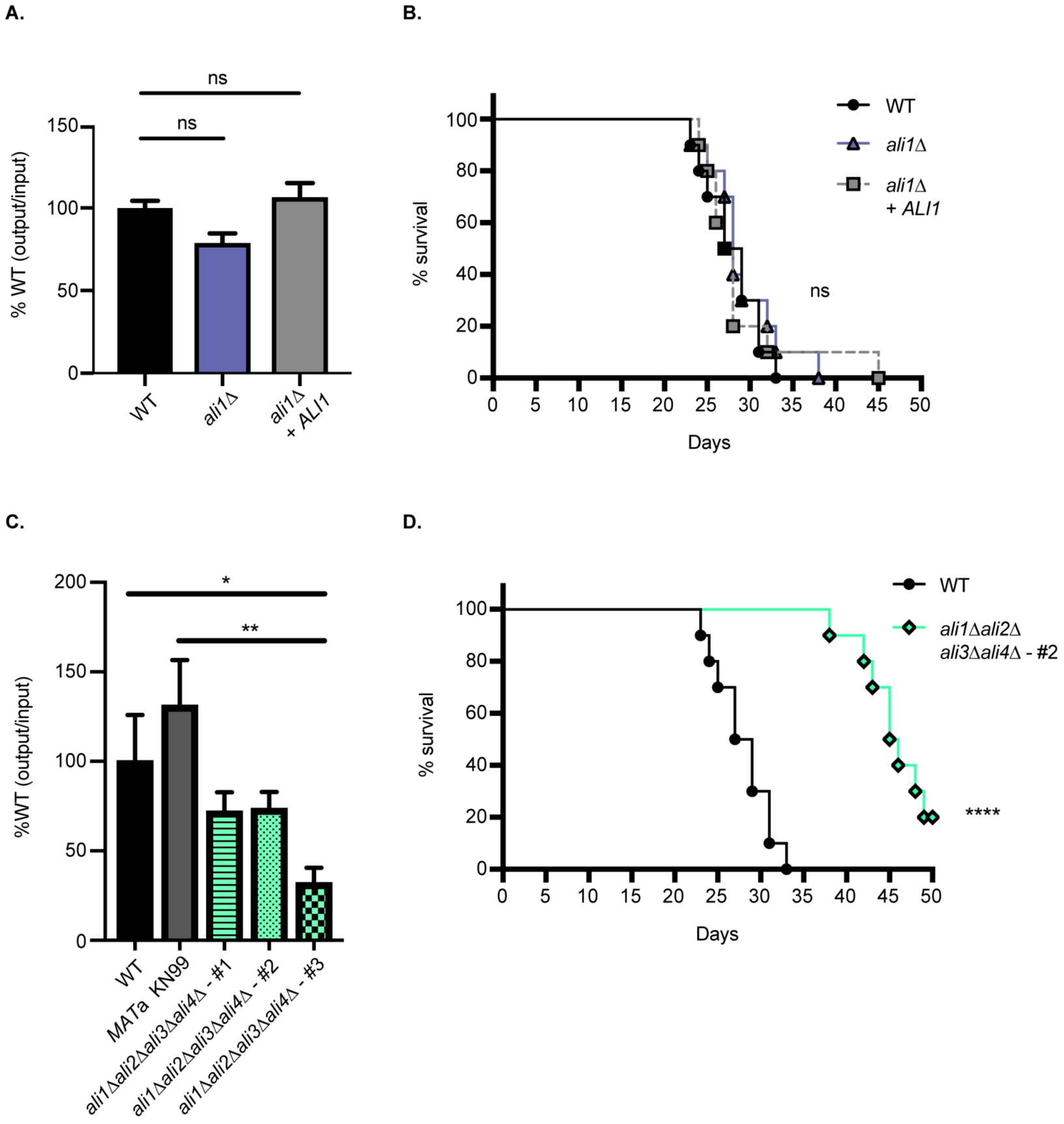

Figure 6

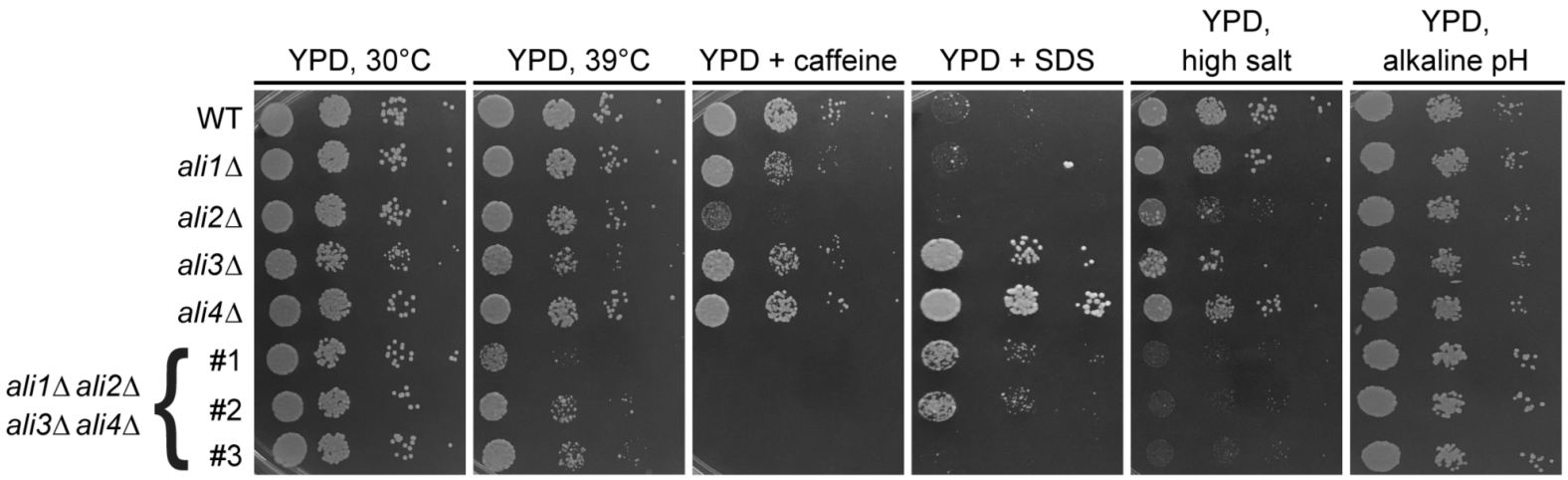

Figure 7